Subglacial Hydrothermal Alteration Minerals in Jökulhlaup Deposits of Southern Iceland, with Implications for Detecting Past or Present Habitable Environments on Mars

Nicholas H. Warner[1] and Jack D. Farmer[2]

Abstract

Jökulhlaups are terrestrial catastrophic outfloods, often triggered by subglacial volcanic eruptions. Similar volcano-ice interactions were likely important on Mars where magma/lava may have interacted with the planet's cryosphere to produce catastrophic floods. As a potential analogue to sediments deposited during martian floods, the Holocene sandurs of Iceland are dominated by basaltic clasts derived from the subglacial environment and deposited during jökulhlaups. Palagonite tuffs and breccias, present within the deposits, represent the primary alteration lithology. The surface abundance of palagonite on the sandurs is 1–20%. X-ray diffraction (XRD) analysis of palagonite breccias confirms a mineral assemblage of zeolites, smectites, low-quartz, and kaolinite. Oriented powder X-ray diffractograms ($<2\,\mu m$ fraction) for palagonite breccia clasts and coatings reveal randomly ordered smectite, mixed layer smectite/illite, zeolites, and quartz. Visible light–near infrared (VNIR) and shortwave infrared (SWIR) lab spectroscopic data of the same palagonite samples show H_2O/OH^- absorptions associated with clays and zeolites. SWIR spectra derived from Advanced Spaceborne Thermal Emission and Reflection Radiometer (ASTER) images of the sandurs reveal $Al-OH^-$ and $Si-OH^-$ absorption features. The identified alteration mineral assemblage is consistent with low temperature (100–140°C) hydrothermal alteration of basaltic material within the subglacial environment. These results suggest that potential martian analog sites that contain a similar suite of hydrated minerals may be indicative of past hydrothermal activity and locations where past habitable environments for microbial life may be found. Key Words: Mars—Reflectance spectroscopy—Astrobiology—Hydrothermal systems—Habitability. Astrobiology 10, 523–547.

1. Introduction

THE MODERN SURFACE OF MARS is unfavorable for life due to the absence of liquid water, the high flux of UV radiation at the surface, and the highly oxidizing nature of the surface regolith. If life exists on Mars today, it is likely to be found in deep subsurface environments where magmatic-hydrothermal systems create habitable zones of sustained liquid water and sources of energy and elemental building blocks needed for life. On Earth, subsurface hydrothermal environments sustain diverse associations of thermophilic microorganisms from all three domains of life (Bacteria, Archaea, and Eukarya). The upper temperature limit for the growth of terrestrial thermophiles is from a hydrogen-utilizing bacterial strain that grows up to 121°C and survives to 130°C (Kashefi and Lovley, 2003). Earth-based studies of geological systems dominated by interactions between molten rock and ice or water, at temperatures below this upper temperature threshold for life, have important applications for astrobiological exploration (Farmer, 1996; Pirajno and van Kranendonk, 2005). Presently, the goal of such studies is to provide robust criteria for recognizing similar processes (past or present) on Mars. Magma-cryosphere interactions appear to have been very important in shaping the martian surface over its history (e.g., Chapman and Tanaka, 2002; Wilson and Mouginis-Mark, 2003a, 2003b; Meresse et al., 2008). The identification of such processes is considered to be key for an accurate assessment of the potential for long-term habitability.

Given the technical challenges associated with deep robotic drilling on planetary surfaces, the search for an extant or extinct subsurface biosphere on Mars may require taking advantage of natural geological processes, such as catastrophic outflows or upwelling hydrothermal systems that

[1]Department of Earth Science & Engineering, Imperial College London, South Kensington Campus, London.
[2]School of Earth and Space Exploration, Arizona State University, Tempe, Arizona.

are capable of bringing deep materials onto the surface. The geomorphic indicators for such environments and processes may be further associated with mineral signatures that are characteristic of hydrothermal activity in the shallow crust. Currently, there is little data confirming the presence of hydrothermal mineral assemblages on the surface of Mars. The observation of opaline silica ($\sim 91\%$ silica) by the Spirit rover represents the best example of a mineralogical identification of hydrothermal activity (Squyres *et al.*, 2008). Spectral mapping from orbit by the Thermal Emission Spectrometer on board Mars Global Surveyor, the Thermal Emission Imaging System on board Mars Odyssey, the OMEGA spectrometer on board Mars Express, and the Compact Reconnaissance Imaging Spectrometer (CRISM) on board the Mars Reconnaissance Orbiter have now identified several minerals that are the products of water/rock interactions (*e.g.*, phyllosilicates, sulfates, Fe oxides, carbonates, halides) and form on Earth over a potentially broad range of pH conditions, temperatures, and water-rock ratios (*e.g.*, Christensen *et al.*, 2001, 2005; Langevin *et al.*, 2005; Bibring *et al.*, 2006; Bishop *et al.*, 2008; Mustard *et al.*, 2008; Osterloo *et al.*, 2008; Poulet *et al.*, 2008). However, much uncertainty remains as to how the general classes of identified minerals relate to specific geological conditions, as the identified spectral characteristics are often not unique to a single mineral, lithology, or geological process (*e.g.*, hydrothermal versus low-temperature weathering alteration processes, impact alteration, evaporative processes).

In the present study, we examined the mineralogical signatures of terrestrial volcano-sedimentary deposits associated with a basaltic volcanic system in southern Iceland.

Similar Icelandic systems have been considered potential analogues for volcano-ice processes on Mars (Rice and Edgett, 1997; Chapman *et al.*, 2003). The study focused on comparing the deposits of two pro-glacial outwash systems (sandur plains) formed by catastrophic outfloods from subglacial volcanic environments. Combining analyses of satellite remote sensing with quantitative ground-truth analyses, we mapped the spatial variability of hydrated mineral signatures over the sandur plains and established the threshold abundances required for the detection of these mineral components, using the available remote data. In addition, we used laboratory techniques to describe the mineral assemblages present on the sandur surfaces to infer the general temperature conditions of alteration. Our analysis indicated that some of the alteration components identified on the sandur plains formed under low-temperature hydrothermal conditions within subglacial environments at temperatures within the range for life. These results may provide a framework for planning future missions to explore for subsurface habitable environments on Mars.

2. Geological Setting and Background

2.1. Icelandic sandur plains

Clifford (1987) first proposed the catastrophic outwash plains (sandurs) of southern Iceland as terrestrial analogues for several catastrophic outflow systems on Mars, including the north and south polar chasmata. Beneath the Vatnajökull glacier in southern Iceland, volcanism associated with the Grimsvötn caldera continuously delivers heat energy that melts substantial volumes of ice (Fig. 1). The meltwater
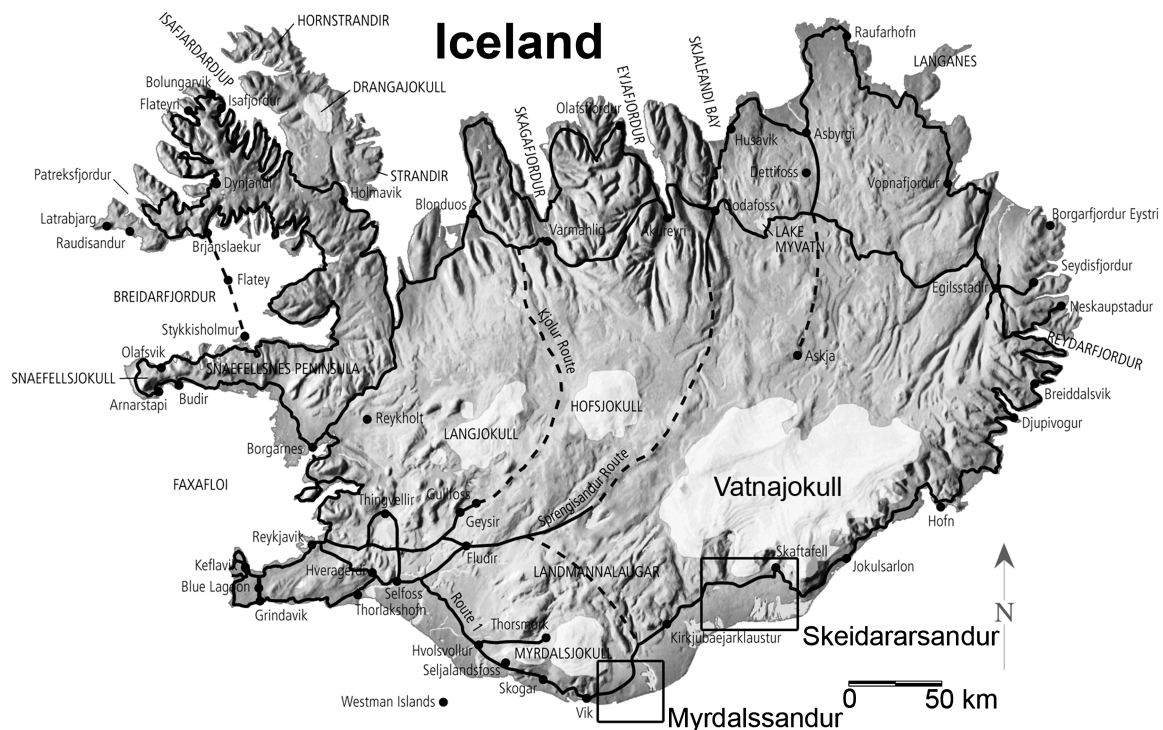

FIG. 1. Location map of Skeiðarársandur and Mýrdalssandur in southern Iceland. Catastrophic floods, sometimes induced by volcanic eruptions beneath the glaciers Vatnajökull and Mýrdalsjökull, provide volcanoclastic sediment to the southern sandur plains.

collects within the Grimsvötn caldera and other subglacial topographic depressions (Gudmundsson and Hognadottir, 2007). The onset of volcanic activity within the Grimsvötn caldera is associated with catastrophic releases of meltwater, due to fracturing and failure of the ice dam that holds the pressurized lake water within the caldera. The resulting catastrophic outflows, known as jökulhlaups, inundate the adjacent outwash plains with meltwater laden with volcanic debris derived from the subglacial lake. Over-pressure and release of water from the caldera lake of the Grimsvötn volcano has occurred on several occasions in response to volcanically induced melting. The most recent outflows occurred in 1996, following eruptions at the nearby Gjálp subglacial fissure (Gudmundsson et al., 1997). This event produced a sediment-laden jökulhlaup (discharge of $10^4 \, \mathrm{m^3 \, s^{-1}}$) that covered the ice-marginal outwash plain of Skeiðarársandur, located directly south of the Vatnajökull ice sheet (Russell et al., 1999; Gomez et al., 2000; Knudsen et al., 2001) (Fig. 1). In addition to juvenile (glass-rich) pyroclastic materials, outflow deposits on the surface of Skeiðarársandur include clasts scoured from subglacially altered bedrock and palagonitic breccias/tuffs that were erupted under the ice and temporarily stored within subglacial depressions.

Approximately 100 km west of Skeiðarársandur, another outwash plain called Mýrdalssandur has been the site of many similar-magnitude catastrophic outflows (discharges of 10^4 to $10^6 \, \mathrm{m^3 \, s^{-1}}$) that originated from beneath Mýrdalsjökull at the Katla subglacial volcanic center (Fig. 1) (Tomasson, 1996). At this locality, the largest magnitude flood in historical times immediately followed the 1918 Katla eruption. This jökulhlaup deposited (on average) an $\sim 8 \, \mathrm{m}$ thick sequence of sand- to granule-sized basaltic glass and pumice over an area of $\sim 400 \, \mathrm{km^2}$ (Maizels, 1993; Duller et al., 2008).

2.2. Palagonite

Preliminary descriptions of the composition of sandur deposits were provided by Maizels (1993), Tomasson (1996), and Duller et al. (2008). These descriptions identified the major alteration lithology on the sandur surfaces as palagonite. In addition, Maizels (1993) identified reworked glacial and volcanic debris within the basal sequences of jökulhlaup deposits. Stefánsdóttir and Gíslason (2005) described the composition of suspended materials in the 1996 Skeiðarársandur outflow. In their analysis, 80% of the suspended sediment was found to be fragments of altered basaltic glass or palagonite, 11% secondary minerals such as zeolites and calcite, and 5% unaltered basaltic glass. Most of the 1996 flood deposits were found to be geochemically similar to products of the Grimsvötn volcanic system. However, only a small sampled fraction was geochemically identical to the 1996 Gjálp eruption materials. This suggests that a large proportion of volcanic debris from the Gjálp eruption remained trapped within the Grimsvötn caldera lake or in nearby subglacial depressions, or both. The major sediment component was therefore likely derived from one or more of the following: (1) older eruptive materials that had previously collected to form basal volcanoclastic sequences within the lake, (2) erosion of subglacial bedrock, (3) reworked fluvial-glacial deposits from the pro-glacial zone of the sandur (Stefánsdóttir and Gíslason, 2005).

Palagonite is a heterogeneous material derived from aqueous alteration of basalt or basaltic glass. It has been defined in various ways in the literature, and the compositional and textural meaning of the term is poorly constrained. Mineralogically and texturally, palagonite has been defined differently as (1) an amorphous hydrated gel (Peacock, 1926), (2) composed of poorly crystalline clays (smectites, illite, kaolinite), in close association with amorphous hydrated phases (Moore, 1966), (3) a yellow-orange hydrated material formed by hydration and devitrification of basaltic glass (Bates and Jackson, 1984), and (4) a chemically heterogeneous hydrated mineral assemblage derived by the hydrothermal or weathering alteration of basaltic glass or lavas (Thorseth et al., 1991).

As an amorphous phase, palagonite consists of light-brown to reddish-brown hydrated Fe oxides. This state is representative of an early stage of alteration that is often typical of low-temperature weathering (Thorseth et al., 1991; Bishop et al., 2002; Drief and Schiffman, 2004; Pokrovsky et al., 2005) and has been assessed at various terrestrial locations as a possible analogue to martian dust (e.g., Allen et al., 1981; Crisp and Bartholomew, 1992; Orenberg and Handy, 1992; Bishop and Pieters, 1995; Roush and Bell, 1995; Bishop et al., 2007; Hamilton et al., 2008). With more-advanced alteration (long-term weathering, or rapid hydrothermal alteration), palagonite can take on an anisotropic character that consists of darker-yellow to brown fibrous (poorly crystalline) materials and leads to increased crystallinity and formation of Fe, Mg-rich clay minerals. The alteration process that changes basalt to palagonite is largely dependent on time, temperature, and the availability of water. Secondary authigenic minerals commonly associated with advanced palagonitization, and often found in basaltic hydrothermal settings, include crystalline zeolites, silica, and calcite (Griffith and Shock, 1995; Bishop et al., 2002). For the present study, we adopted the general definition of palagonite given by Thorseth et al. (1991), noting specific changes in crystallinity, composition, and appearance that reflect varying degrees of alteration.

3. Methods

3.1. Field analysis

Field work was conducted at Skeiðarársandur and the adjacent sandur plain, Mýrdalssandur, during the summers of 2006 and 2007. Outflow deposits from the pre-1890, 1938, and 1996 Skeiðarársandur floods, and the 1918 jökulhlaup at Mýrdalssandur were identified based on geomorphological and stratigraphic relationships compiled by Maizels (1993), Gomez et al. (2000), Russell and Knudsen (2002), and Duller et al. (2008). Figure 2 shows the locations of surface samples taken at both sandurs. Samples were collected from the upper 5 cm of the sandur surface within $1 \times 1 \, \mathrm{m}$ quadrats. Sand- to pebble-sized sandur materials were collected and point counted in the lab to determine absolute lithologic abundances. Point counting of 1–5 g of fine (silt-sand) samples was conducted under a binocular microscope with gridded sample slides. For each sample, the percent lithologic abundances were assigned. Counting error was determined only for the palagonite clasts by counting each sample twice. For each count, the difference in estimated palagonite abundance was found to be $\pm <1$–3%. The counts included the following
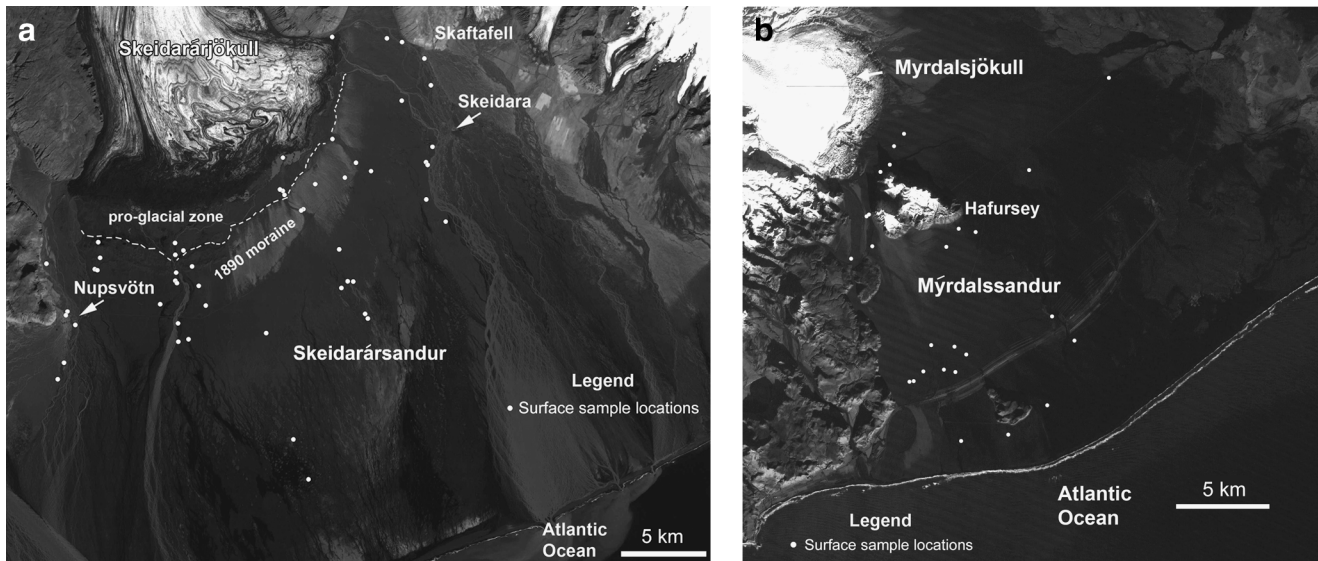
FIG. 2. Visible light ASTER images of (**a**) Skeiðarársandur and (**b**) Mýrdalssandur showing the location of surface samples and quadrats taken from outflow sediment.

lithologic categories: (1) palagonite, (2) highly vesicular basalt (50–70% vesicles by surface area), (3) moderately vesicular basalt (30–50%), (4) poorly vesicular basalt (10–30%), (5) dense basalt (<10%), and (6) other materials, which included intermediate to felsic volcanics (andesites, dacites, rhyolites) and mineral separates (albite, quartz, zeolites, etc.). The percent vesiculation of basaltic clasts was determined by visually estimating the surface area of a single clast covered by vesicles. This information was used only as a means by which to evaluate the potential for significant vesicle infill of secondary alteration materials (*e.g.,* clays, zeolites, silica), which, when included with the clast abundances of palagonite, would likely increase the total surface area abundance of hydrated materials exposed on the sandur plains.

In regions where the clast size was too coarse (cobble to boulder) to collect and return to the lab, surface quadrats were documented with scaled-referenced digital images. These regions included proximal localities within the Skaftafell National Park along the eastern boundary of Skeiðarársandur, localities along the Nupsvötn River at the western boundary of Skeiðarársandur, and sites within the immediate pro-glacial zones at both sandurs. In total, 83 surface quadrats were sampled on the sandur surfaces, including one image for each location where hand samples were acquired (Fig. 2). Each quadrat digital image contains color information that was used to extract lithologic surface area abundance data. The commercial image processing tool Adobe Photoshop was used to isolate pixels of specific colors from each image. For the abundance determination, we assumed that all pixels within the provided histogram that were within the yellow-tan-orange color range represent palagonite clasts. This assumption was supported by our point-counting lithologic analysis and from field observations. The color extraction process was done iteratively until all pixels within the selected color range were removed. This method left any identifiable palagonite clast transparent in the original base image. Clasts of different colors (red, white, green), which are representative of minor lithologies, were present in both the point-counted samples and the images at

abundances of <2%. The total percent of the pixels extracted from the image was used to determine the percent area on the surface occupied by palagonite clasts (surface area abundance). The colored pixels of palagonite were pasted to a new blank white image to display the clast distribution on the surface. Palagonite abundances at the sample locations (with GPS coordinates) were mapped on background geo-referenced satellite images acquired from the Advanced Spaceborne Thermal Emission and Reflection Radiometer (ASTER) to illustrate potential surface abundance patterns.

3.2. X-ray diffraction

X-ray powder diffraction was used to determine the mineralogy of sandur materials and assess the accuracy of remote sensing spectral analyses. X-ray diffractograms were obtained by a Siemens D-5000 diffractometer with a 7.5° wide position-sensitive detector. The incident beam was CuKα radiation (40 kV, 30 mA) with a 1.0 mm antiscatter slit. A nickel foil was used to limit the beta lines for copper. No monochromator was used. Powders for bulk analysis were initially crushed to <0.4 mm in a McCrone percussion mortar and pestle. The sample was surrounded with corundum pucks in the mortar to prevent direct contact between the pestle and the sample. Three grams of each sample was weighed with the addition of 0.333 g of ZnO standard. This standard was used for quantitative analysis of randomly oriented bulk powder diffractograms. The sample was further crushed to <20 μm in a McCrone micronizing mill with 4 mil of ethanol for 5 minutes. The crushed sample was rinsed with ethanol and dried overnight at 60°C. The dried sample was then sieved through a 20 μm mesh and loaded into an aluminum slide mount to create a random distribution of powdered sample for analysis. Randomly oriented powders were run over a 2θ range of 5–65° at 0.02° step intervals, with a step time of 2 seconds. This method helped to bring out the crystalline peaks over the background intensity that is generated by amorphous phases like volcanic glass or nanophase Fe oxides, which dominated sandur

samples. Major mineral phases were identified with the X-ray diffraction (XRD) software; Jade and relative mineral abundances were quantified with the Microsoft Excel based program RockJock (Eberl, 2003). RockJock compares integrated XRD intensities of a sample to that of a defined standard. The program utilizes the Solver function in Excel to analyze a given pattern and match the intensities to specific minerals. The percent abundance of each mineral is then determined from the proportion of each chosen standard that is required in combination to make a best fit to the pattern. A degree-of-fit parameter is given for each run sample.

For those samples deemed likely to contain clay minerals, oriented mounts of $<2\,\mu m$ powders were prepared for analysis. Samples subjected to this type of analysis were primarily the palagonitic clasts. In addition, palagonite coatings on pumice clasts were subsampled for the clay analysis. Figure 3 illustrates scanning electron microscope images and photographs of palagonite-coated pumice clasts. The coatings on these clasts are ~ 10–$50\,\mu m$ thick but may be thicker where palagonite infills vesicles or absent between vesicles. To remove the coatings from the basaltic pumice, samples were sonicated in 40 ml of distilled water. The suspended fluid was then emptied into a 40 ml test tube and spun in a centrifuge at 2500 rpm for 5 minutes. The upper clear water layer containing Cl ions was poured off (to prevent flocculation), and the samples were sonicated and spun again at 2500 rpm for 3–5 minutes. This step was repeated until the clear layer was no longer present. The samples were then sonicated and run at 750 rpm for 3.23 minutes to separate the $<2\,\mu m$ fraction. After each run, the suspended fraction that contained the $<2\,\mu m$ fraction was poured off into a beaker. The material was allowed to settle overnight, after which the upper fluid of suspended material was poured off. The remaining liquid was extracted and placed on a glass slide. To reveal the presence of expandable clays (smectites) in the diffractograms, one sample was air dried overnight at 60°C, and the other was dried overnight at 60°C in the presence of ethylene glycol. Each sample was run from 5–30° 2θ at 0.02° steps, with a 2-second step time. The resulting diffractograms were compared to patterns produced for standard oriented clay samples (air dried and glycolated) with use of the results from the NEWMOD computer program presented in Moore and Reynolds (1997). Quantitative determination of absolute abundances of clays with Rock-Jock is not possible via this method. However, we were able to obtain valuable information about the relative abundances of specific clay minerals.

3.3. Lab spectroscopy

As a supplement to the XRD data, visible light–near infrared/shortwave infrared (VNIR/SWIR) lab spectra were also obtained from sandur materials to determine mineralogy (including amorphous Fe oxides and hydrated glasses that are not recognizable in the XRD analysis). For this analysis, 80 surface samples were collected from the sandur plains. A full-range ASD VNIR/SWIR lab spectrometer was used to characterize the samples over a wavelength range of 0.35–2.5 μm with the use of a halogen lamp for illumination and a spectralon reference panel. The ASD spectrometer has a 5 nm spectral resolution over the spectral range 0.35–1.0 μm and 11 nm spectral resolution from 1.0 to 2.5 μm. For each bulk sand sample or clast subsample, 20 spectra were acquired and averaged. Offsets between internal spectrometers were corrected, and spectra were converted to absolute reflectance by using a NIST traceable spectralon reflectance spectrum. Corrected spectral averages were converted to a binary format, compatible with the United States Geological Survey (USGS) spectral software program SPECPR to allow comparisons to mineral spectra in the USGS spectral library. Corrected data were also written as independent .ascii files for display with the remote sensing and image analysis software package ENVI. ENVI contains USGS and Jet Propulsion Laboratory spectral libraries that were further used to compare spectral features.

3.4. ASTER remote sensing

Visible light–near infrared and shortwave infrared ASTER images were obtained for Skeiðarársandur and Mýrdals-sandur from the Earth Observing System data gateway (AST_07), which contains atmospherically corrected surface reflectance data at 15 m resolution for 3 bands in the VNIR (0.52–0.86 μm) and 30 m resolution for 6 bands in the SWIR (1.60–2.43 μm) (Fujisada, 1995) (Table 1). Atmospheric correction of the ASTER images, provided with the AST_07
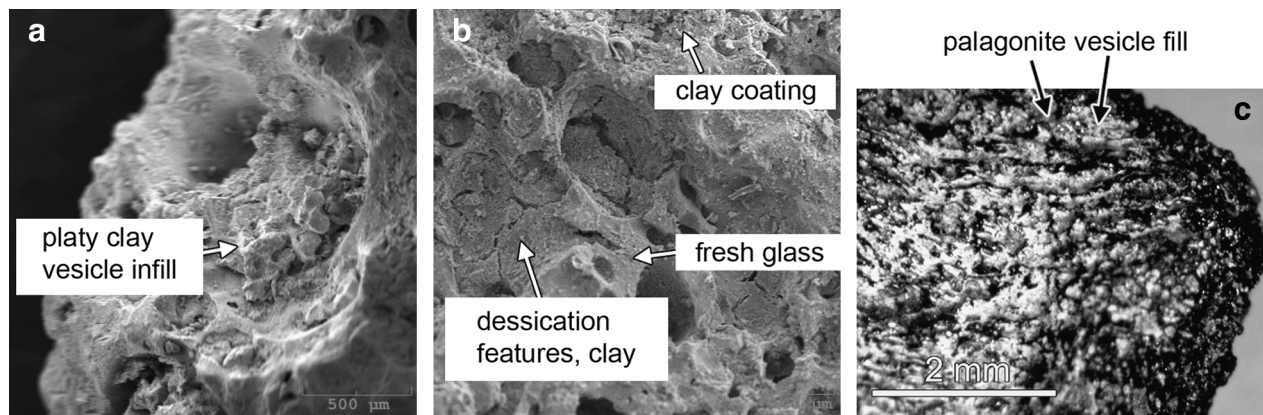

FIG. 3. (**a, b**) Scanning electron microscope images and (**c**) photograph of a clast of palagonite-coated basaltic pumice taken from Mýrdalssandur. The images illustrate the thin (10–50 μm) coating of clay-sized palagonite that commonly surrounds and fills the vesicles of sandur clasts.

TABLE 1. ASTER VNIR-SWIR BANDPASSES AND RESOLUTION

Band label		Wavelength (μm)	Resolution
B1	VNIR band 1	0.52–0.60	15 m
B2	VNIR band 2	0.63–0.69	15 m
B3	VNIR band 3N	0.76–0.86	15 m, Nadar view
B4	VNIR band 3B	0.76–0.86	15 m, Backward scan
B5	SWIR band 4	1.60–1.70	30 m
B6	SWIR band 5	2.145–2.185	30 m
B7	SWIR band 6	2.185–2.225	30 m
B8	SWIR band 7	2.235–2.285	30 m
B9	SWIR band 8	2.295–2.365	30 m
B10	SWIR band 9	2.36–2.43	30 m

data, requires input information regarding atmospheric absorption/scattering and radiance from the surface and atmosphere. The atmospheric correction algorithm applied by the Earth Observing System data gateway utilized a look-up table containing parameters for the satellite, sun, and atmosphere. These parameters included the solar zenith angle, satellite view angle, azimuth angle between the sun and satellite, molecular scattering optical depth, aerosol scattering optical depth, aerosol scatter albedo, aerosol size distribution, and surface reflectance. The resulting ASTER data were converted from radiance at the sensor to atmospherically corrected reflectance from the surface.

Lab and field analyses of mineral components within the sandur materials were directly compared to the remote data for each collection site, which thus provided the means by which to assess the validity of the identifications made via ASTER. The SWIR range (1.60–2.43 μm) is ideal for the identification of hydrothermal alteration minerals, owing to the presence of absorption features related to OH^-, H_2O, and $(CO_3)^{2-}$ molecular vibrations (Hunt, 1977; Rowan and Mars, 2003). For this analysis, two ASTER scenes were obtained over southern Iceland, one displaying the outwash plain at Skeiðarársandur and the other at Mýrdalssandur. Two methods were utilized to map the mineralogy of the sandur surfaces. These included (1) Spectral Angle Mapper (SAM) classification and (2) spectral unmixing/matched filtering. Similar techniques have been used by Rowan and Mars, (2003), Rowan *et al.* (2003), and Rowan *et al.* (2004) to describe the mineralogy of hydrothermal deposits and ultramafics with the use of spectral data from ASTER and the Airborne Visible/Infrared Imaging Spectrometer.

3.4.1. Spectral Angle Mapper method.
The SAM algorithm allows for supervised classification of multispectral/hyperspectral reflectance data with user-defined spectral classes (end members) that are used to match unknown materials on an image (Kruse *et al.,* 1993; Rowan and Mars, 2003). With this method, the known and unknown spectra are plotted as vectors in n-dimensional space, the spectral angle between the two classes is calculated, and a match is made by using a given threshold angle. Because the algorithm only utilizes the vector direction in its calculation, this method is insensitive to surface illumination that is illustrated by the vector length. To generate a SAM classification image of the sandur plains, an Iceland sandur spectral library was constructed by using lab spectroscopic data obtained

from the ASD lab spectrometer. While such prior knowledge of the composition of some remote surfaces (*i.e.,* Mars) is not available, a similar method can be applied with a set of possible or likely reference spectra. For our analysis, each chosen sandur spectrum was convolved to ASTER spectral resolution in ENVI for use as the reference spectra for the SAM classification. Specific lab spectra showing absorption features related to basaltic alteration and the presence of possible hydrothermal mineral components (OH^- and H_2O absorptions) were selected as the end-member spectra and matched with the SAM algorithm to unknown spectra by using the ENVI threshold Single Value option and an angle threshold of 0.1 radians. Classification images were generated to display the most likely matches to the chosen reference spectra on the images.

3.4.2. Spectral unmixing method.
Spectral unmixing techniques were also applied with the software package ENVI. This method varies from SAM in that spectral end members were not selected from measured data but were determined from algorithms that are designed to identify spectrally pure pixels on the image. Segregation and removal of noise in the scene was initially required to reduce the computational time for the unmixing algorithms. The Minimum Noise Fraction Transformation (MNF) function, a Principal Component-type analysis, was applied to reduce the noise in the data sets. In our analysis, the transformation generated 6 new band images from the original 6-band SWIR image, where images with a high signal/noise represented MNF bands 1, 2, and 3. These bands were selected by visual inspection of the resultant MNF images and from two-dimensional plots of the MNF bands (*e.g.,* MNF band 1 vs. MNF band 2). The low-noise MNF bands were used to identify spectrally pure pixels with the Pixel Purity Index (PPI) algorithm (Kruse *et al.,* 1993; Rowan *et al.,* 2004). The PPI function determines the number of times a given pixel in n-dimensional space can be considered extreme relative to other pixels in the scene. The PPI was processed at 1000 iterations and with a threshold of 3. The output image highlights those pixels that are considered extreme. Extreme pixels were plotted in n-dimensional space by using ENVI's N-D Visualizer to reveal groups of unique end-member pixels. The end-member pixels were mapped and displayed on the images. Spectral end members determined by this process were displayed on the images by using the Mixed Tuned Matched Filtering (MTMF) function in ENVI. The MTMF algorithm maximizes the response of the known end member and displays this response on the image. In our analysis, red, green, and blue were assigned to represent the locations of the three identified end members.

4. Results

4.1. Field analysis

Figure 2 shows the locations of scoop samples and quadrat images taken from the surfaces of Skeiðarársandur and Mýrdalssandur. Table 2 provides example results of the clast point counts from sand-sized surface materials deemed unsuitable (too fine) for digital image abundance mapping. From the point count results, field observations, and the digital image color extraction, the dominant alteration lithology identified on the sandur plains is palagonite (Fig. 4). Figure 5

TABLE 2. EXAMPLE GRAIN POINT COUNT DATA FOR COARSE-FINE SAND-SIZED SURFACE SAMPLES
AT SKEIÐARÁRSANDUR AND MÝRDALSSANDUR

Sample ID	High vesicular basalt (%)*	Mod. vesicular basalt	Low vesicular basalt	Dense basalt	Palagonite	Other
Skeiðarársandur						
060701.1A	7	21	14	46	6	6
060701.5A	25	14	11	42	3	5
060702.6B	23	13	9	46	4	3
060703.3B	6	14	30	35	4	8
060703.4B	25	14	18	34	5	4
060703.5B	3	12	27	50	5	1
060703.6A	10	11	19	40	19	1
060705.3B	28	16	18	31	5	2
Average	16	14	18	36	6	4
Mýrdalssandur						
060708.1B	28	8	45	16	2	1
060708.5B	67	14	6	11	1	1
060708.6B	41	15	15	10	17	1
060708.9B	22	26	11	23	16	2
060713.2B	44	21	10	17	6	1
060713.3B	94	0	0	5	1	0
Average	49	14	15	14	7	1

*Percent surface area of vesicles: High vesicular = 50–70%; Mod. vesicular = 30–50%; Low vesicular = 10–30%; Dense = <10%.

displays example image quadrats with color data removed to display the surface area abundance of palagonite on the sandur surface. The palagonitic clasts for both sandurs vary in composition and texture. The majority of palagonitic clasts represent volcanic breccias (palagonite breccias), specifically, aggregates of angular aphanitic and glassy basalt surrounded by highly altered yellow-orange, basaltic glass (hyaloclastites). Some palagonite clasts are fine grained and represent only the altered basaltic glass component (palagonite tuffs).

Advanced Spaceborne Thermal Emission and Reflection Radiometer (ASTER) VIS images were used as base maps to illustrate the surface area abundance and spatial distribution of palagonite on the sandur surfaces determined in the field and in the lab by the point counting and digital image color extraction techniques (Fig. 6). At Skeiðarársandur, palagonite is in highest abundance (>5%) within the pro-glacial zone and along bedrock outcrops. Exposed along the bordering cliffs to the east of the river Skeiðara and to the west of the river Nupsvötn, these bedrock exposures contain 0–5 million-year-old layered sequences of subglacially erupted volcanics, subaerially erupted lavas, and glacio-fluvial sediments deposited during inter-glacial periods (Helgason and Duncan, 2001). Massive to layered sequences of palagonitic breccias and hyaloclastites exposed within the outcrops are the source of the palagonite-rich zones on the sandur. These materials were likely reworked by floods from localized skree and fan deposits at the base of the cliffs. At Mýrdalssandur, palagonite abundances ranged from <1% to ~20%. The highest palagonite abundances (~20%) were observed south of Hafursey, a palagonite-rich bedrock remnant located proximal to the margin of Katlajökull.

4.2. X-Ray diffraction

X-ray diffraction (XRD) techniques using powdered samples of sandur materials were used to determine the mineralogy of sandur surfaces and evaluate variability in composition of
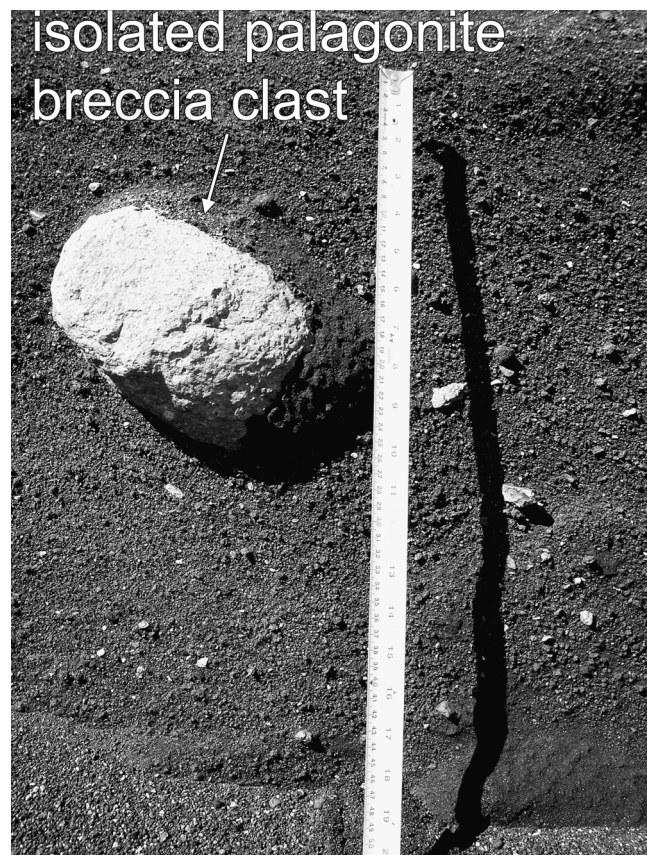

FIG. 4. Photograph of a cobble-sized (~10 cm) clast of palagonite breccia surrounded in a matrix of sand- to granule-sized basaltic pumice within 1918 catastrophic outflood deposits at Mýrdalssandur. Yellow-orange palagonite breccia clasts are the most common alteration material present on the surface of the sandur deposits and occur in abundance of 1–20% by surface area.
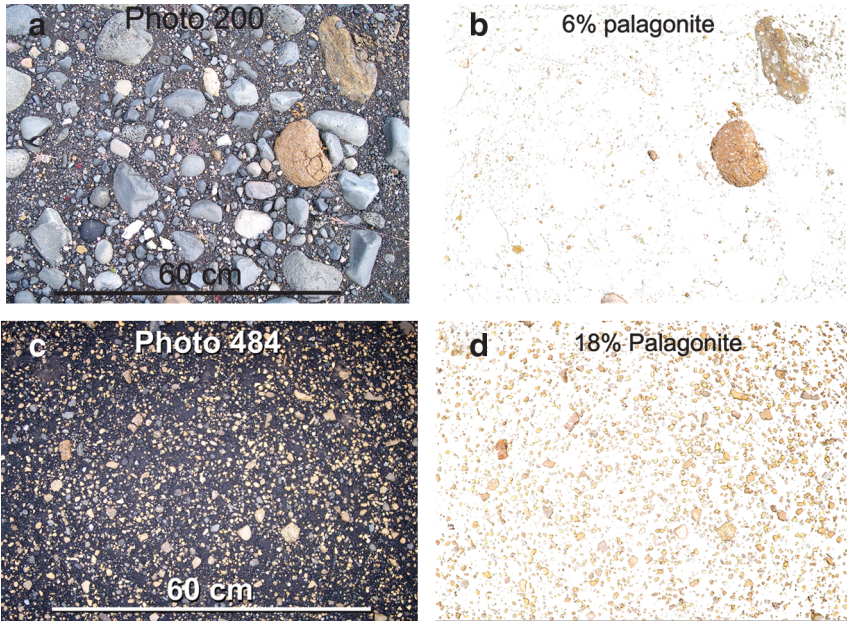
FIG. 5. Example surface quadrats from (**a**, **b**) Skeiðarársandur and (**c**, **d**) Mýrdalssandur. Quadrat images were acquired for coarse surfaces and were used to estimate the abundance (by surface area) of palagonite clasts within the deposits (b, d). Photos c and d were obtained from Mýrdalssandur on a surface that contains the highest abundance of palagonite of any location on the sandur plains.

the palagonite clasts. X-ray diffractograms were obtained from surface samples of sandur mixtures and from basaltic pumice clasts, palagonite clasts, and palagonite coatings. Bulk sandur, random powder diffractograms contain crystalline peaks of plagioclase feldspar (best fit to albite), pyroxene, and a minor peak for smectite (Fig. 7a). Maximum intensity peaks for plagioclase and pyroxene occur at 2θ values of $27.76°$ and $29.72°$, respectively. The bulk sandur diffractogram is consistent with a glass-rich basaltic material,

with a minor smectite clay component that is likely derived from palagonite clasts/coatings.

The basaltic pumice (basalt clast) diffractogram, collected from the 1918 Mýrdalssandur deposit, shows significant background intensity related to amorphous volcanic glass, with minor intensity peaks for plagioclase (albite), low-quartz, and pyroxene (Fig. 7b). The quartz in these basaltic pumice samples was present as fill in vesicles and fractures. The plagioclase was identified as microlites and phenocrysts within the basalts. Yellow-tan palagonite coatings were
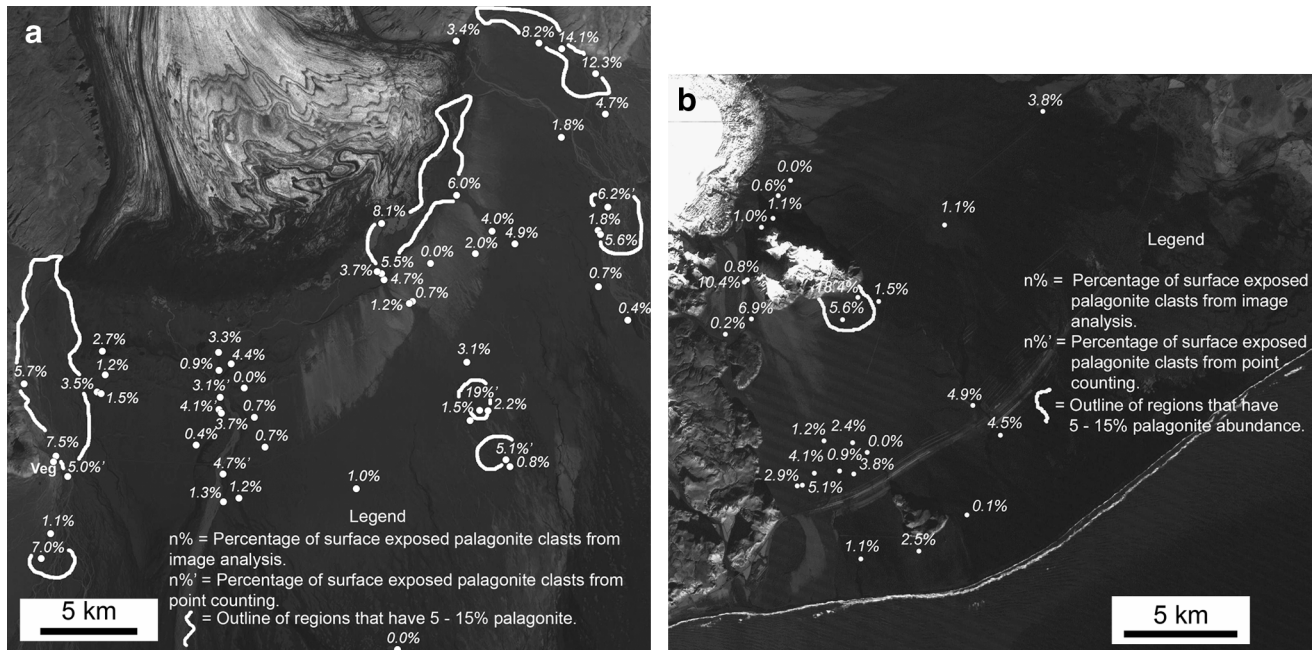

FIG. 6. ASTER visible light images displaying the field/lab-mapped abundances of surface palagonite on (**a**) Skeiðarársandur and (**b**) Mýrdalssandur. The highest abundance of palagonite (5–20%) was mapped at bedrock proximal localities along the east and west banks of Skeiðarársandur and south of the bedrock remnant Hafursey at Mýrdalssandur.
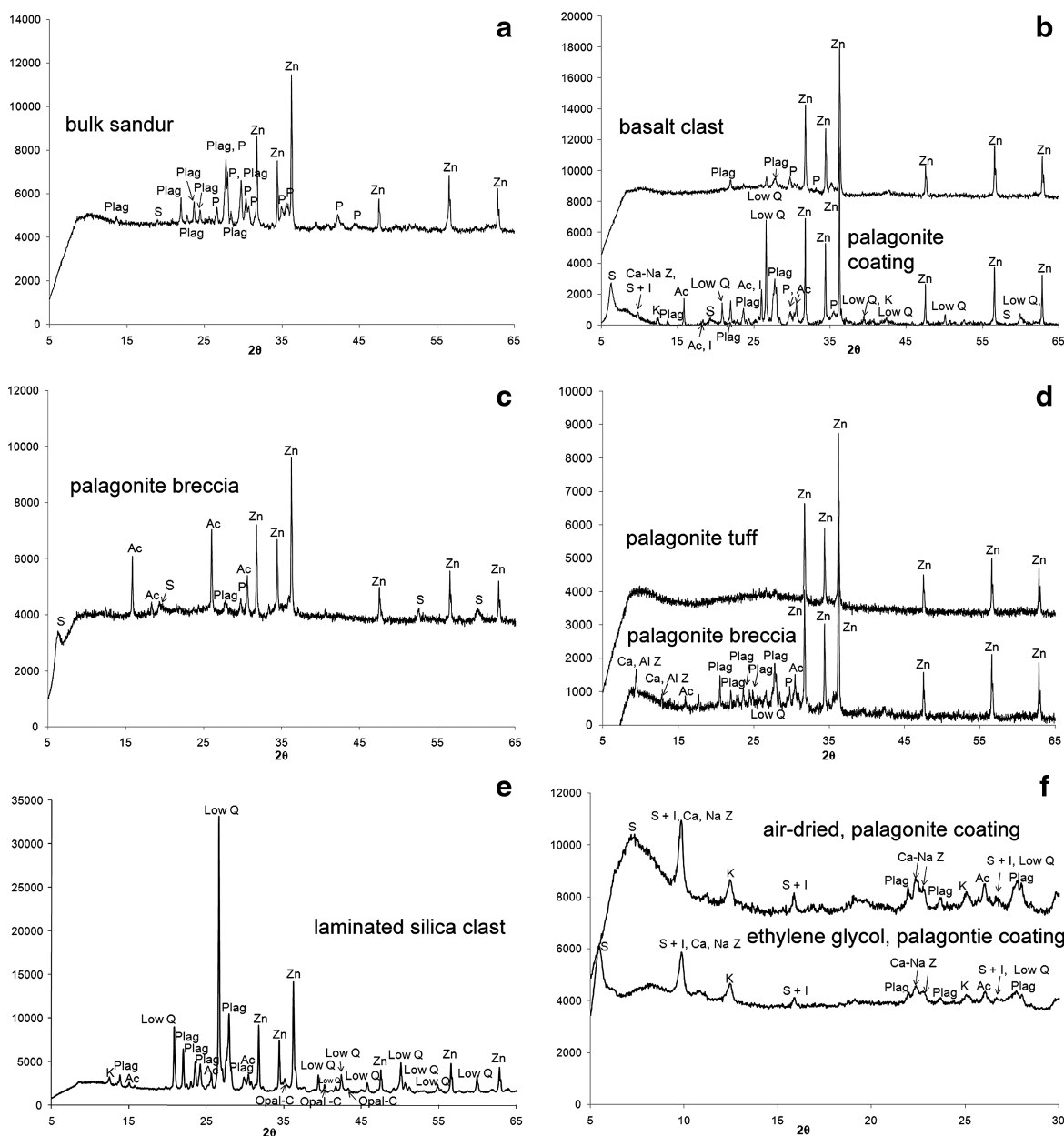
FIG. 7. X-ray powder diffractograms of (**a**) a bulk sample of outflow deposits at Skeiðarársandur, (**b**) a fresh basaltic clast and palagonite coating (counts offset for clarity) at Mýrdalssandur, (**c**) a sample of a single palagonite breccia clast from Skeiðarársandur, (**d**) a clast of palagonite tuff and palagonite breccia (counts offset for clarity) from Hlöðufell (tuya), and (**e**) a clast of laminated silica from Skeiðarársandur. Plate (**f**) displays the air-dried and glycolated oriented powder diffractograms of the clay-sized (<2 μm) fraction of a palagonite coating acquired from Mýrdalssandur. Mineral symbols on the peaks are plagioclase (Plag), pyroxene (P), low-quartz (Low Q), illite (I), smectite (S), kaolinite (K), analcime (Ac), calcium-sodium zeolites, *e.g.,* heulandite or stilbite (Ca-Na, Z), calcium-aluminum zeolites, *e.g.,* laumontite (Ca-Al, Z), opal C (Opal-C), and the zincite standard (Zn).

common on most of the basaltic pumice clasts at Mýrdalssandur (Fig. 3). These coatings were likely emplaced during late stage settling of clay-sized particulates following the outflood event. The random powder diffractogram for the palagonite coatings shows maximum 2θ intensity peaks for crystalline low-quartz at 20.82°, plagioclase feldspar (albite) at 27.74°, smectite clay at 6.2°, analcime at 15.84°, Ca, Na-rich zeolites (heulandite or stilbite) at 9.74°, and pyroxene at 29.72°. Minor peaks for illite and kaolinite are also present.

Depending on the conditions of basalt alteration, the abundance of crystalline hydrated mineral phases in palagonite varies, which alters the intensity and location of X-ray peaks. There is, therefore, no single defining diffraction pattern for palagonite. Figure 7c is an X-ray diffractogram for an example palagonite breccia clast collected from Skeiðarársandur. Crystalline smectite and analcime peaks are obvious in the sample analysis, but there is significant background intensity related to amorphous and nanophase Fe
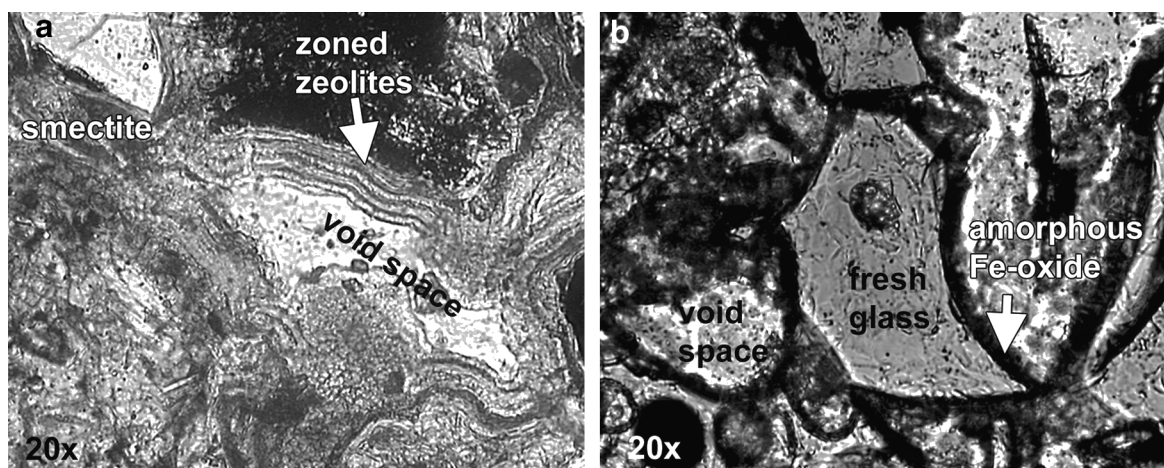
FIG. 8. Plane-light thin sections of (**a**) a palagonite breccia clast from Hlöðufell displaying authigenic void-filling zeolites and smectites (**b**) a palagonite tuff clast from Hlöðufell displaying Fe oxide alteration rims surrounding fresh basaltic glass.

hydroxides (Moore and Reynolds, 1997). Such amorphous materials are common alteration products of basaltic glass and are difficult to analyze via standard XRD methods (Bishop *et al.*, 2002). Their presence in palagonite samples challenged peak identifications. However, the majority of palagonite clasts collected from the sandurs consisted of highly crystalline mineral phases with distinctive 2θ peaks for both primary basaltic minerals (feldspars, pyroxene, etc.) and secondary alteration minerals (*e.g.*, zeolites, silica, and clays).

For comparisons with sandur palagonitic materials, X-ray diffractograms were acquired for palagonite breccias and palagonite tuffs collected from bedrock exposures at the base of the Pleistocene-aged Hlöðufell tuya (subglacial volcano) in central Iceland (Fig. 7d). Petrographic thin sections of the palagonite breccias (Fig. 8) showed vein and vesicle fills containing zoned zeolites that were likely comprised of varying ratios of Na and Ca. Similar to the palagonite breccia clasts collected on the sandur plains, the XRD analyses of the tuya breccia clasts revealed abundant secondary authigenic zeolites, including laumontite and analcime. However, results of XRD analyses of palagonite tuffs collected from Hlöðufell lack any evidence for crystalline phases, including clays or zeolites. Thin sections taken of these palagonitic tuffs show only thin Fe-oxide coatings surrounding unaltered volcanic glass, similar to fine-grained palagonite tuff samples collected from Skeiðarársandur and Mýrdalssandur (Fig. 8).

Mineral abundances in the random powder analysis were determined by using the relative intensities of the ZnO peaks in the program RockJock (Eberl, 2003) (Table 3). However, matching standards were unavailable for zeolite minerals, nontronite clay, and amorphous/nanophase Fe oxides-hydroxides in this program. As a result, the total computed abundance for the palagonite and bulk sandur samples only reaches ~50% with a degree of fit of ~0.3 for the pattern match (a degree of fit of 0 is a perfect match). The missing 50% includes the Fe oxides-hydroxides, zeolite minerals, and unaltered glass. Basaltic glass standards from Hekla volcano in Iceland were available in RockJock. The program did not find a match with this standard for any of the analyzed sandur samples. To test RockJock's ability to match standards, a glass-poor sample collected from Skeiðarársandur

was analyzed. Figure 7e displays the diffractogram of the hand sample, described as a finely laminated, silica-rich clast, collected along the west bank of the Skeiðara River. The XRD pattern obtained from this sample shows peaks for low-quartz, opal-c, plagioclase (albite), kaolinite, and analcime. This clast was likely derived from an alkaline, low-temperature siliceous hydrothermal system that was active beneath the current Vatnajökull ice cap or an earlier predecessor. Compositionally similar silica-rich hydrothermal systems are present at many locations throughout Iceland (Arnórsson, 1975, 1983; Kristmannsdóttir and Tómasson,

TABLE 3. MINERAL ABUNDANCES FOR SPECIFIC SANDUR SAMPLES FROM THE ROCKJOCK QUANTITATIVE XRD ABUNDANCE TECHNIQUE

Mineral standards	Bulk sandur abundance (%)	Palagonite breccia: sandur	Laminated light clast: sandur
low-quartz	1	7.5	11
opal (Virgin co.)	0	0	4.2
opal-CT	0	0	0
opal 282	0	0	3.1
Chert	0	0	29
Plagioclase	28	27	50
Pyroxene	11	4	0
Kaolinite	0	0	2.1
Saponite	3.4	9.7	0
Chlorite	0	0.9	0
Illite	0	0	0
Montmorillonite	0	0	0
Hekla glass	0	0	0
nontronite*	?	?	?
analcime*	?	?	?
heulandite*	?	?	?
stilbite*	?	?	?
amorphous Fe oxides/hydroxides*	?	?	?
Total	43%	49%	99%
Total Unknown	57%	51%	1%

*Standard pattern not available in RockJock.

1978; Jakobsson and Moore, 1986; Griffith and Shock, 1995). The Rock Jock analysis of this siliceous clast identified plagioclase as the major component at 50% abundance, chert at 29%, low-quartz at 11%, opal at 7.3%, and kaolinite at 2.1% (Table 3). The total unknown in this sample is $\sim 1\%$ with a ~ 0.0 value for degree of fit (near perfect match). This result indicates that the RockJock mineral identification function and quantification closely matches XRD results in cases where matching standards are available in the program.

From the clay analysis of palagonite coatings ($<2\,\mu m$ fraction), Figure 7f displays air dried and glycolated diffractograms from 5–30° 2θ. The expansion of smectite minerals in the ethylene glycol sample shifted the location of the maximum 001 smectite peak from 7.2° 2θ in the air-dried sample to 5.42° 2θ in the glycolated sample. The position of the 001 smectite peak for the glycolated sample indicates $R < 1$, or random ordering (Moore and Reynolds, 1997). Mixed layered smectite/illite peaks are present at 2θ values of 9.80°, 15.86°, and 26.14°. The $\Delta 2\theta$ value for the 002/003 (15.86° 2θ) and 001/002 (9.80° 2θ) illite/smectite peaks suggests 30–40% illite (Moore and Reynolds, 1997). Kaolinite peaks or chlorite peaks, or both, are present at 12.40° 2θ and 24.98° 2θ. Non-clay mineral peaks were identified by pattern matching with diffractograms of oriented air-dried and glycolated samples produced by the NEWMOD computer program (Moore and Reynolds, 1997). A low-quartz peak overlaps with illite/smectite at 26.14° 2θ and may be present in the sample. Plagioclase peaks are present at 2θ values of 21.94°, 23.62°, and 27.72°. The 100% intensity peak for the zeolite mineral heulandite overlaps with the illite/smectite peak at 9.82° 2θ. Other identifiable heulandite peaks in this sample occur at 22.32° and 22.72° 2θ. An analcime peak is visible at 25.98° 2θ.

4.3. Lab spectroscopy

Visible light–near infrared–shortwave infrared spectra were obtained for 80 samples collected from Skeiðarársandur and Mýrdalssandur. Figure 9 displays four example spectra of sandur materials acquired from 0.35–2.5 μm. The lowermost spectrum represents a typical, sand- to granule-sized (2ϕ to -2ϕ) bulk sandur mixture containing abundant basaltic material and a minor amount (5%) of palagonite. A broad absorption feature near 1.0 μm is typical of pyroxene (the reader is referred to Clark et al., 1990; Clark, 1999; Bishop et al., 2002 for example library spectra of major mineral groups). A small feature with an absorption minimum at 1.89 μm represents the H_2O bend and OH^- stretch combination bands (Clark et al., 1990; Clark, 1999; Bishop et al., 2002). All sandur samples were oven dried at 40°C to remove exterior moisture, while preventing significant desiccation of clays. The feature near 1.9 μm likely represents bound H_2O in clay, or possibly zeolite minerals present as authigenic phases in the palagonite clasts. The low reflectance of the sample is typical of all sand- to granule-sized dark (low-albedo) sandur mixtures.

The spectrum labeled aphanitic basalt in Fig. 9 was acquired from an individual cobble-sized basaltic clast collected from the surface of the Nupsvötn outflow channel at Skeiðarársandur. Typical of individual basaltic clasts, the spectrum has a low reflectance and shows few distinct absorption features in this spectral range. The broad absorption feature near 1.0 μm suggests pyroxene. In contrast to the bulk
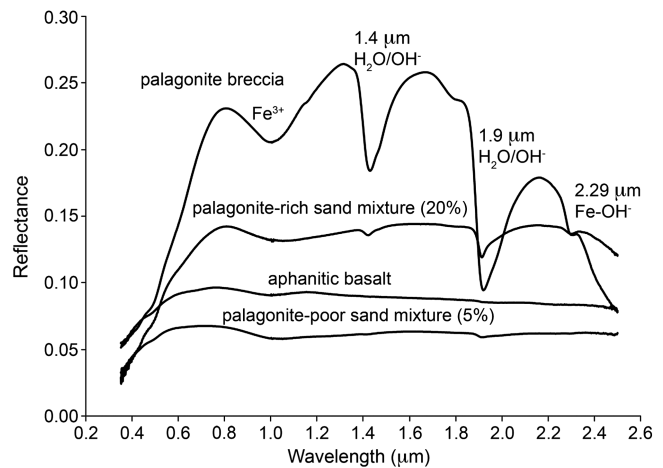

FIG. 9. Lab spectra (VNIR-SWIR) of a palagonite breccia clast and sandur mixtures containing different abundances of palagonite. A nonlinear mixing relationship is obvious with the sandur spectra. These samples contain palagonite surrounded in a fresh, unaltered basaltic matrix. Absorption features related to H_2O-OH^- bound minerals (clays or zeolites) can be identified in the lab for samples with >5% abundance of palagonite (abundance determined from point count analysis).

sandur sample, which contains a trace amount of palagonite, no 1.9 μm feature is present in the aphanitic basalt spectrum.

The spectrum labeled palagonite-rich sandur mixture (Fig. 9) was collected from the Mýrdalssandur outflow plain, south of the Hafursey bedrock remnant. This sand- to granule-sized mixture contains the highest abundance of palagonitic clasts ($\sim 20\%$) identified on either sandur plain and, thus, exhibits a higher absolute reflectance relative to the basalt-dominated samples of similar clast size. The spectrum exhibits a broad feature at 1.0 μm and three sharp absorption features with absorption minima at 1.40, 1.90, and 2.29 μm. The 1.40 μm feature represents the first overtone band of the OH^- stretching mode (Clark et al., 1990; Clark, 1999; Bishop et al., 2002). The presence of this band and the depth of the 1.90 μm feature indicate that the palagonite-rich sample contains a higher abundance of H_2O and OH^- bound minerals relative to the palagonite-poor and aphanitic basalt samples. The appearance of the 2.29 μm feature is consistent with Fe-OH^- bearing nontronite clay (Clark et al., 1990; Clark, 1999; Bishop et al., 2002).

Finally, the spectrum with the highest absolute reflectance was acquired from a single cobble-sized palagonite breccia clast (Fig. 9). This sample was collected along the west bank of the Nupsvötn River, and the spectrum contains absorption features attributable to H_2O-OH^- bound minerals and Fe-OH^- minerals (Clark et al., 1990; Clark, 1999; Bishop et al., 2002). Aside from a narrower absorption feature near 1.0 μm and a general broadening of the 1.4 and 1.9 μm features that resulted from a mixture of H_2O/OH^- bearing phases (zeolites and clays), the spectral shape of the palagonite clast sample is similar to the palagonite-rich sandur mixture spectrum. Narrowing of the 1.0 μm band, with a band minima of 0.98 μm, is consistent with the presence of Fe^{3+}, which is likely related to nanophase/amorphous (e.g., ferrihydrite) or crystalline Fe oxides (Clark et al., 1990; Clark, 1999; Bishop et al., 2002).

The shape and location of absorption features between 2.0 and 2.3 μm can be used to determine the relative abundance of Al, Fe, and Mg in a clay-rich sample (Clark *et al.,* 1990; Clark, 1999; Bishop *et al.,* 2002). Diagnostic features in this range can be used to infer the presence of specific clay minerals. This method is often preferred over XRD clay analysis, where overlapping peaks may obscure identification (Clark, 1999). Figure 10 displays the 1.8–2.4 μm range of two example palagonite breccia clasts collected on the sandur plains. In Fig. 10a, the single distinct absorption feature present at 2.29 μm is diagnostic of di-octahedral clay, nontronite (Fe-OH⁻). Substitution of Mg for Fe in the clay structure shifts absorption features in this range from 2.29 to 2.31 μm (Clark *et al.,* 1990; Clark, 1999; Bishop *et al.,* 2002). Absorption features at 2.31 μm are indicative of saponite, a tri-octahedral smectite mineral (Fe, Mg-OH⁻). The majority of palagonite samples identified in this analysis exhibit absorptions at 2.29 μm, which indicates the dominance of nontronite. However, 2.31 μm features are also present in analysis results of some samples.

a 0.146

20% palagonitic clast abundance, sandur mixture

1.9 μm
H₂O/OH

2.29 μm
nontronite clay
Fe-OH

b 0.0640

5% palagonitic clast abundance, sandur mixture

1.9 μm
H₂O/OH

2.20 μm 2.24 μm   2.29 μm

2.20 μm = illite or montmorillonite
2.24 μm = hydrated silicate glass
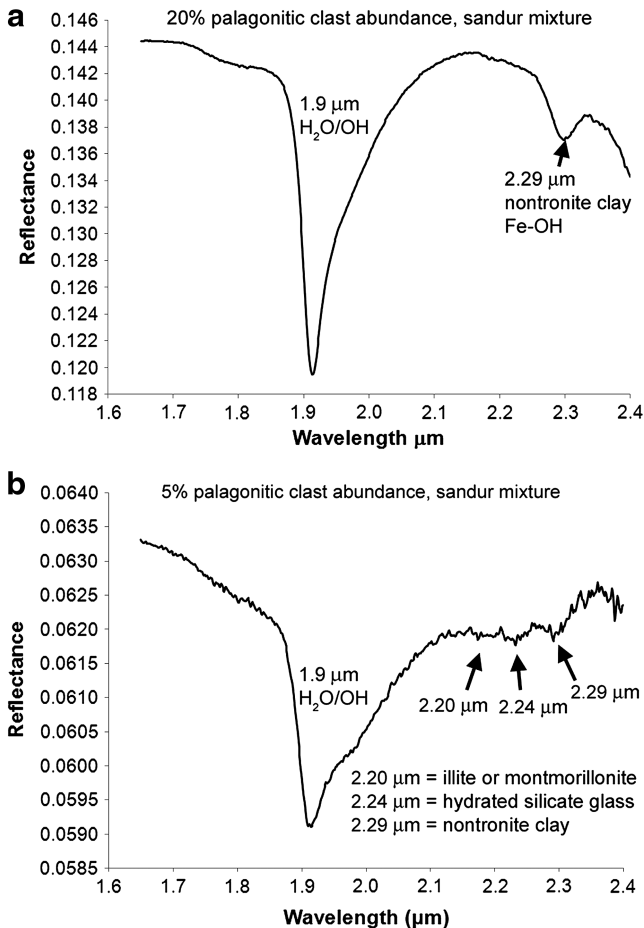2.29 μm = nontronite clay

FIG. 10. Lab spectra showing only the SWIR range (1.6–2.4 μm) of the sandur mixtures displaying important absorption features related to nontronite clay (2.29 μm), illite/montmorillonite (2.20 μm), and hydrated silica (2.24 μm). The depth of the clay absorption feature in the sandur mixtures that contain a palagonite abundance of 5% is resolvable at the limit of the background noise.

X-ray diffraction (XRD) analysis results suggest the presence of other clay minerals in the palagonite clasts, including illite and kaolinite. Figure 10b highlights two additional absorption features that are common to sandur palagonite samples and basaltic sand mixtures that contain palagonite. The presence of a narrow 2.20 μm absorption feature is typical of vibrational overtones from the Al-OH⁻ molecule and is consistent with montmorillonite or illite (Clark *et al.,* 1990; Clark, 1999). In addition, the absorption feature at 2.24 μm may be related to hydrated silica (Si-OH⁻). Terrestrial weathering of basaltic lava flows under arid conditions commonly produces hydrated silica rinds through nonlinear, time-dependent diffusion of water, which results in the small 2.24 μm feature (Swayze *et al.,* 2007). This process represents an early stage of weathering alteration that likely occurs on the youthful Icelandic sandur surfaces. Such processes have also been postulated for Mars (Kraft *et al.,* 2007; Minitti *et al.,* 2007).

The presence of crystalline zeolite minerals in sandur palagonite clasts is indicated by 2θ peaks for heulandite, stilbite, and analcime phases in the diffractograms. Zeolites are found in sandur palagonite breccia clasts as both amygdules and vein fills (Fig. 8). Vein-filling materials were isolated from a palagonite breccia clast for further spectroscopic analysis. Figure 11a displays the spectrum of heulandite collected from this sample. Figure 11b is a photograph of the sampled zeolite vein within a palagonite breccia clast. A shoulder in the spectrum at 0.59 μm and a broad absorption feature with a band minimum of 0.97 μm are consistent with the presence of Fe^{3+}. Small absorptions at 0.97 and 1.15 μm have been identified in zeolite samples related to OH⁻/H₂O combination and overtone bands (Cloutis *et al.,* 2000). A weak absorption feature at 1.15 μm is present in the heulandite sample. The 0.97 μm feature may be present but overlaps with Fe^{3+} absorption bands that may be related to Fe-oxide contamination in the zeolite sample (mechanical contamination from the extraction of zeolites from the palagonite clast). The deep absorption features at 1.42 and 1.91 μm are consistent with structural OH⁻ and absorbed, or bound, H₂O. The feature near 1.4 μm in zeolite samples contains two distinct absorption bands at 1.42 and 1.47 μm (Cloutis *et al.,* 2000). The deeper 1.42 μm feature is the result of combinations and overtones of OH⁻ stretching fundamentals at 2.76 and 2.81 μm. A shoulder at 1.47 μm is present in the Iceland zeolite sample. Similar to the 1.4 μm feature, the absorption near 1.9 μm was described by Cloutis *et al.* (2000) to contain two resolvable features, including a strong absorption band at 1.91 μm and a weaker band at 1.98 μm. A small shoulder at 1.94–1.96 μm is resolvable in Fig. 11a and can be attributed to the combination of these two bands. The strong 1.91 μm band is the result of the combination of OH⁻ stretching fundamentals at 2.76–2.81 μm and the 6.1 μm H₂O bending fundamental. A shoulder near 2.3–2.4 μm may be related to clay contamination in the sample or a result of OH⁻ stretching fundamentals described in zeolite samples in Cloutis *et al.* (2000).

4.4. ASTER remote sensing results

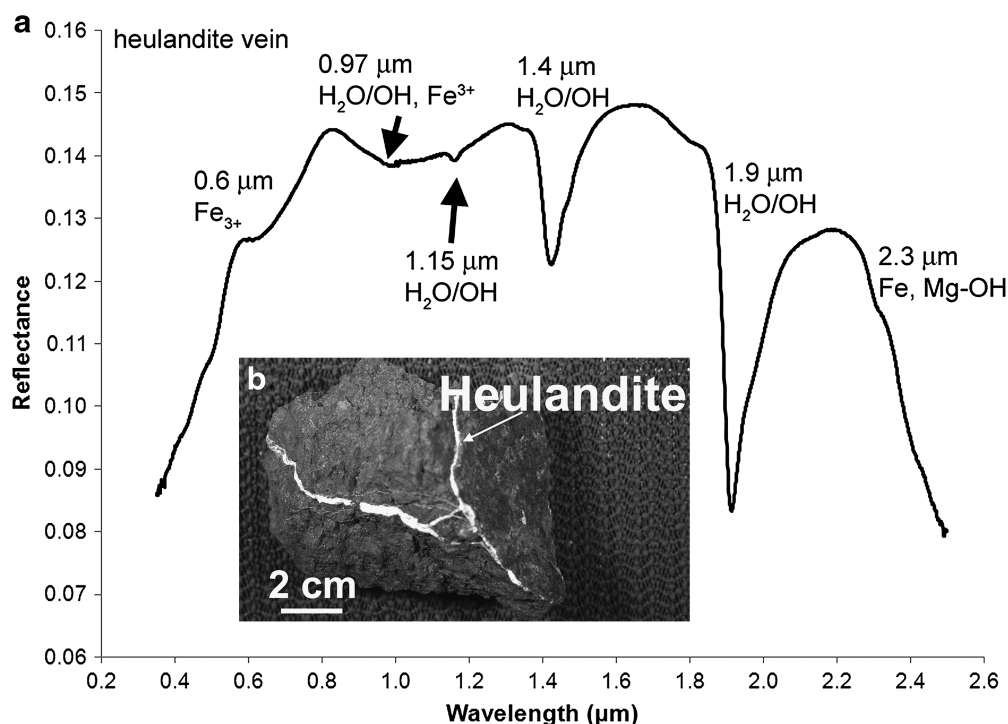4.4.1. *Spectral Angle Mapper results.* The presence of altered basaltic material (palagonite) is obvious in the field.

FIG. 11. (**a**) Lab spectra (VNIR-SWIR) of a heulandite (Ca, Na zeolite) vein from a palagonite breccia clast sampled at Hlöðufell. Absorption features related to H_2O and OH^- and typical of zeolites are present at 0.97, 1.4, and 1.9 μm. Overlap of these features with absorption features typical of clay minerals challenges the detection/distinction of single mineral phases in palagonites. (**b**) Photograph of palagonite breccia clast with zeolite vein.

As noted previously, palagonitic clast abundances vary from <1% to 20%, depending on the location on the sandur plain (Fig. 6). ASTER VNIR and SWIR images were obtained for the sandur plains for remote spectral analysis. For the SAM analysis, lab spectra acquired from sandur samples were convolved to ASTER spectral resolution. Figure 12 highlights the lab and ASTER-convolved SWIR spectra for three samples collected on the sandur. Each lab spectrum contains absorption features related to H_2O/OH^- at 1.9 μm and clay absorptions or hydrated silica absorptions from 2.2 to 2.4 μm. Due to the location of the ASTER band filters (Table 1), the 1.9, 2.29, and 2.31 μm features are not represented in the

ASTER-convolved spectra. The 2.29 and 2.31 μm features are diagnostic of nontronite and saponite clay, respectively, which, on the sandur plains, are markers of palagonitized materials. ASTER therefore is unable to remotely identify these clays on the sandur plains. Absorption features at 2.20 and 2.24 μm that are related to $Al-OH^-$ (possibly illite or montmorillonite) and $Si-OH^-$ (hydrated glass) are present in ASTER-convolved spectra and therefore can be mapped in ASTER images. Based on powder XRD techniques, illite was identified in this analysis as a component of palagonitized basaltic materials. These spectral features, although associated with multiple alteration phases in geologically diverse
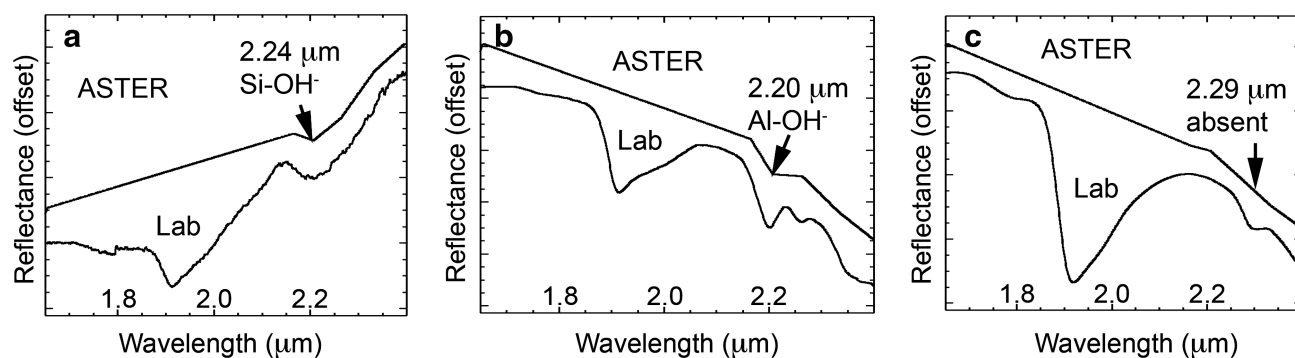

FIG. 12. SWIR lab spectra of sandur mixtures convolved to ASTER resolution. The illite/montmorillonite $Al-OH^-$ (2.20 μm) and hydrated silica $Si-OH^-$ (2.24 μm) absorption features are preserved in the convolution; however, the nontronite/saponite clay $Fe/Mg-OH^-$ (2.29, 2.30 μm) absorptions are removed. ASTER detection of palagonite clasts on the sandur plains is therefore limited to the detection of illite and hydrated silica. These minerals are not exclusive to palagonite but, in the basalt-dominated sandur system, are likely markers of the palagonite alteration assemblage.

environments on Earth and Mars, serve as an indicator on the sandur plains of altered basalt (palagonite).

ASTER-convolved spectra that show the indicators for basalt alteration identified above were selected as end members and used to generate SAM classification images. Figure 13a is a SAM classification image of the Skeiðarársandur outflow plain. Green pixels represent match locations for spectra that contain the 2.20 μm absorption feature tracking Al-OH⁻ absorptions. Red pixels represent the best matches for spectra that show the 2.24 μm feature tracking Si-OH⁻ absorptions. End-member matches occur at Skeiðarársandur within glacial proximal and bedrock proximal zones, including the western bank of the Nupsvötn River and the eastern bank of the Skeiðara River. Few matches were identified within the distal sandur, and no matches correspond with areas of high vegetation, as indicated through field comparisons with occurrences of thick grasses and moss-like vegetation. Evidence of basalt alteration is also present in the ASTER data in outcrop exposures along the western flanks of the Skaftafell Mountains on the eastern border of Skeiðarársandur. Field reconnaissance of the bedrock exposures at Skaftafell revealed an abundance of subglacial volcanic materials, including palagonite breccias, tuffs, pillow basalts, and tabular lava flows. Comparison of the digital image abundance mapping and point count results with the SAM classification image showed a strong correlation between regions on the sandur where high palagonite abundances were observed within cobble-boulder-rich flood deposits and where there are spectral matches that indicate basalt alteration (Figs. 6 and 13). This result suggests that ASTER is capable of identifying altered basaltic material on a surface dominated by unaltered basaltic clasts (basaltic glass, pumice, and lava). Such an observation is relevant to current Mars spectral observations, which have begun to identify evidence for hydrated mineral phases in basalt-dominated terrains (*e.g.,* Christensen *et al.,* 2001, 2005;
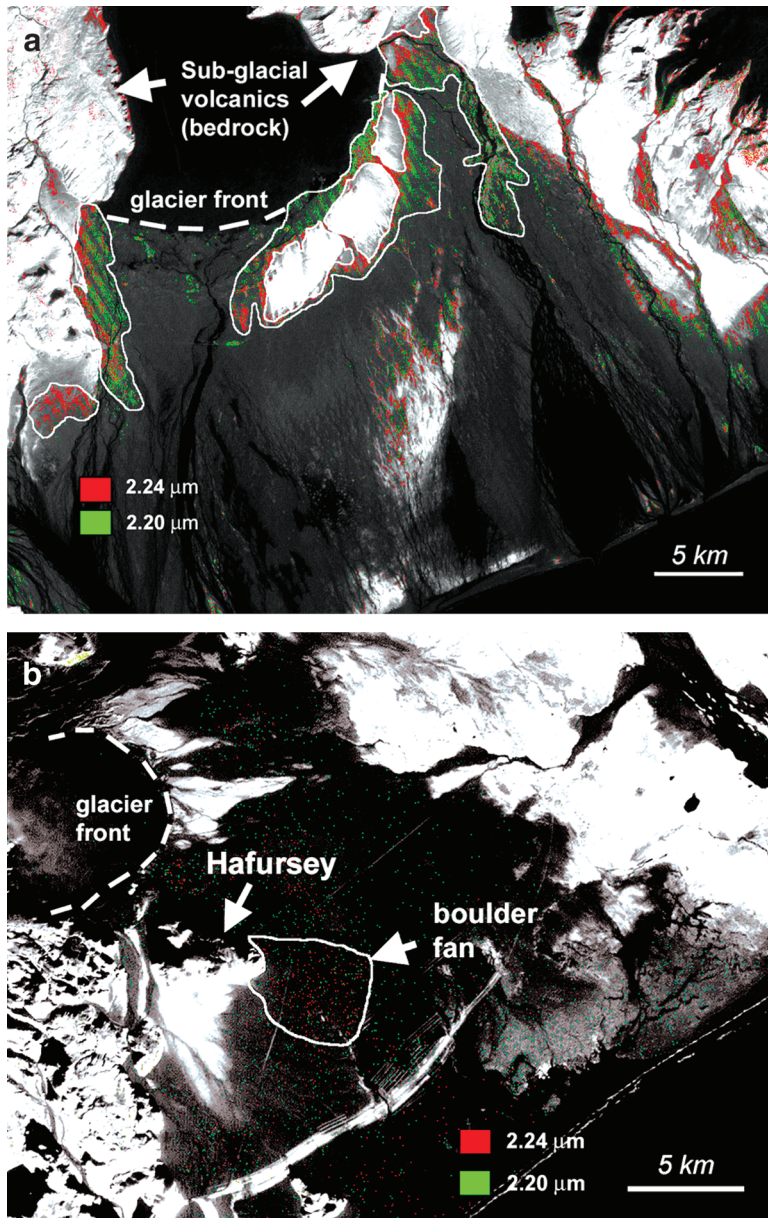

FIG. 13. SAM classification results (displayed over ASTER MNF band 1 base image) from (**a**) Skeiðarársandur and (**b**) Mýrdalssandur showing the distribution of spectral matches to the 2.20 and the 2.24 μm absorption features. The highest density of spectral matches corresponds with the proximal pro-glacial zone and bedrock proximal localities at Skeiðarársandur. A higher density of spectral matches is evident south of the Hafursey bedrock remnant at Mýrdalssandur. This result is in good agreement with the field-mapped abundances of palagonite clasts on both sandurs (see Fig. 6).
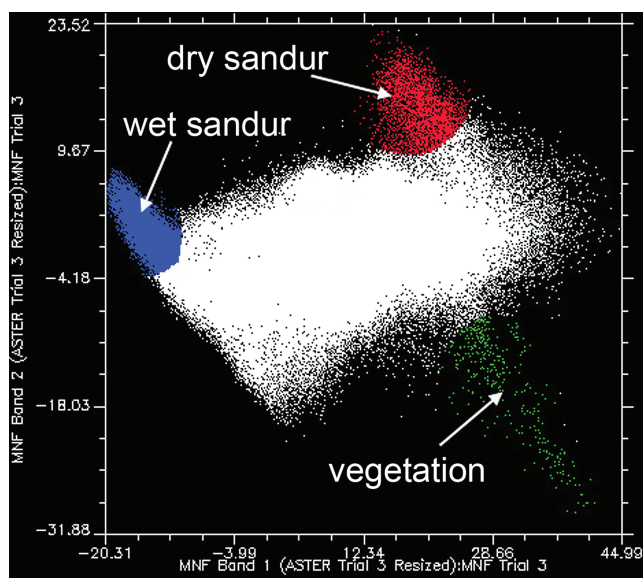
FIG. 14. A two-dimensional visualization (MNF band 1 vs. MNF band 2) of the ASTER spectral data at Skeiðarársandur displaying three distinct end members corresponding to dry sandur materials (red), wet sandur materials (blue), and vegetation (green). These end members were mapped by using the MTMF function and are displayed in Fig. 15.

Langevin *et al.,* 2005; Bibring *et al.,* 2006; Bishop *et al.,* 2008; Mustard *et al.,* 2008; Osterloo *et al.,* 2008; Poulet *et al.,* 2008). However, basic remote identifications of Al-OH$^-$ and Si-OH$^-$ on other remote surfaces can only be used as first-order indicators of the process of alteration in the absence of field data. Similar signatures are possible under multiple aqueous alteration conditions of materials that have a broad range of silicate compositions. For the Iceland case presented here, field analysis revealed palagonite as the likely alteration phase, although ASTER failed to identify spectral signatures

of Fe, Mg-rich clays that are important products of the hydration of basaltic materials.

Figure 13b is a SAM classification image of Mýrdalssandur that shows the best pixel matches for the 2.20 μm features (green pixels) and 2.24 μm features (red pixels). Aside from a large concentration of matches for the 2.24 μm feature behind the Hafursey bedrock remnant, no obvious spatial relationships for alteration are present at Mýrdalssandur. The overall homogeneous distribution of palagonite on the surface of this sandur may explain the remote observations. Field mapping at Mýrdalssandur revealed a relatively low abundance of palagonite clasts across the outwash plain (<5%) with an outlier of high palagonite abundance within a boulder field south of the Hafursey bedrock remnant (Fig. 6). This observation may explain the concentration of Al-OH$^-$, Si-OH$^-$ spectral matches in that region (Fig. 13). However, particle size effects may also play a role in this identification (see Section 5.1).

4.4.2. *Spectral unmixing results.* Spectral unmixing techniques revealed three distinct end-member spectra for the Skeiðarársandur outflow plain. Figure 14 shows a two-dimensional visualization (MNF band 1 vs. MNF band 2) of the spectral data. The average spectrum for each data cloud was taken and given a specific color for representation on the image. Figure 15 is a MTMF classification image of western Skeiðarársandur that designates the three end members for image representation. Based on ground truth observations, the end members correspond closely with locations of vegetated surfaces (shown in green), areas covered in water (shown in blue), and dry sandur materials (shown in red). Results from the spectral unmixing procedure failed to identify unique aqueous alteration bands that can be tied to specific minerals for those surfaces covered by vegetation or standing water. The dry sandur end-member spectrum, however, shows a distinct absorption feature related to Al-OH$^-$ at 2.20 μm.
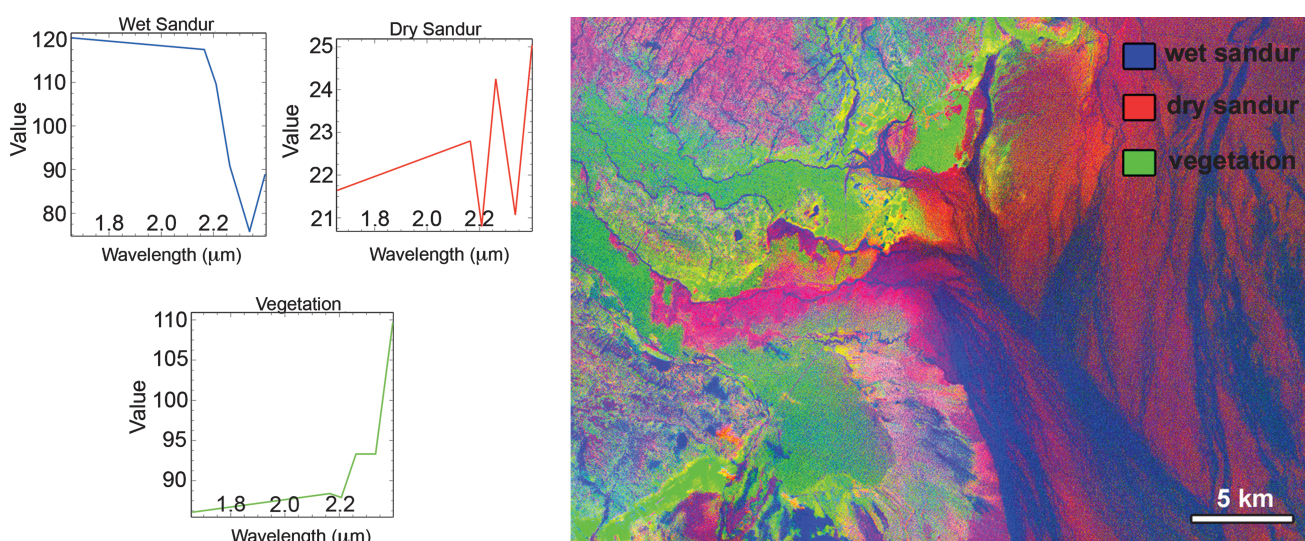

FIG. 15. A MTMF classification image of Skeiðarársandur and example ASTER spectra displaying the three spectral end members identified in Fig. 14. The red regions correspond to dry sandur deposits. The blue and green areas correspond to wet sandur materials and regions with extensive vegetation coverage, respectively. This classification is in general agreement with field observations and was used to identify regions for surface sampling.

5. Discussion

5.1. Palagonite identification and hydrothermal alteration

Palagonitized basalts are common constituents of sandur deposits, which make up <1 to 20% of the clasts exposed on the surface. In addition, an unquantifiable amount of vesicular clasts on the sandur surfaces contain amygdules of palagonite, silica, and zeolites. Nearly 50% of the juvenile pumice clasts derived from the 1918 eruption at Katla on Mýrdalssandur exhibit 50–70% vesicles by surface area, of which several surface exposures and gully outcrops revealed

secondary coatings of clay-sized palagonite. Palagonite clasts likely originated from erosion of subglacial volcanic units present at the base of the glaciers, from bedrock exposures bounding the margins of sandurs, and from primary geothermal zones within the active subglacial volcanic centers. The composition and texture of the identified palagonite varies and is likely controlled by the variety of alteration conditions that are present within the subglacial volcanic system (Allen *et al.*, 1981; Thorseth *et al.*, 1991; Bishop *et al.*, 2002). Figure 16 is a cross-section schematic through an example subglacial volcano or tuya, which illustrates common stratigraphic relationships. Also included in Fig. 16 are
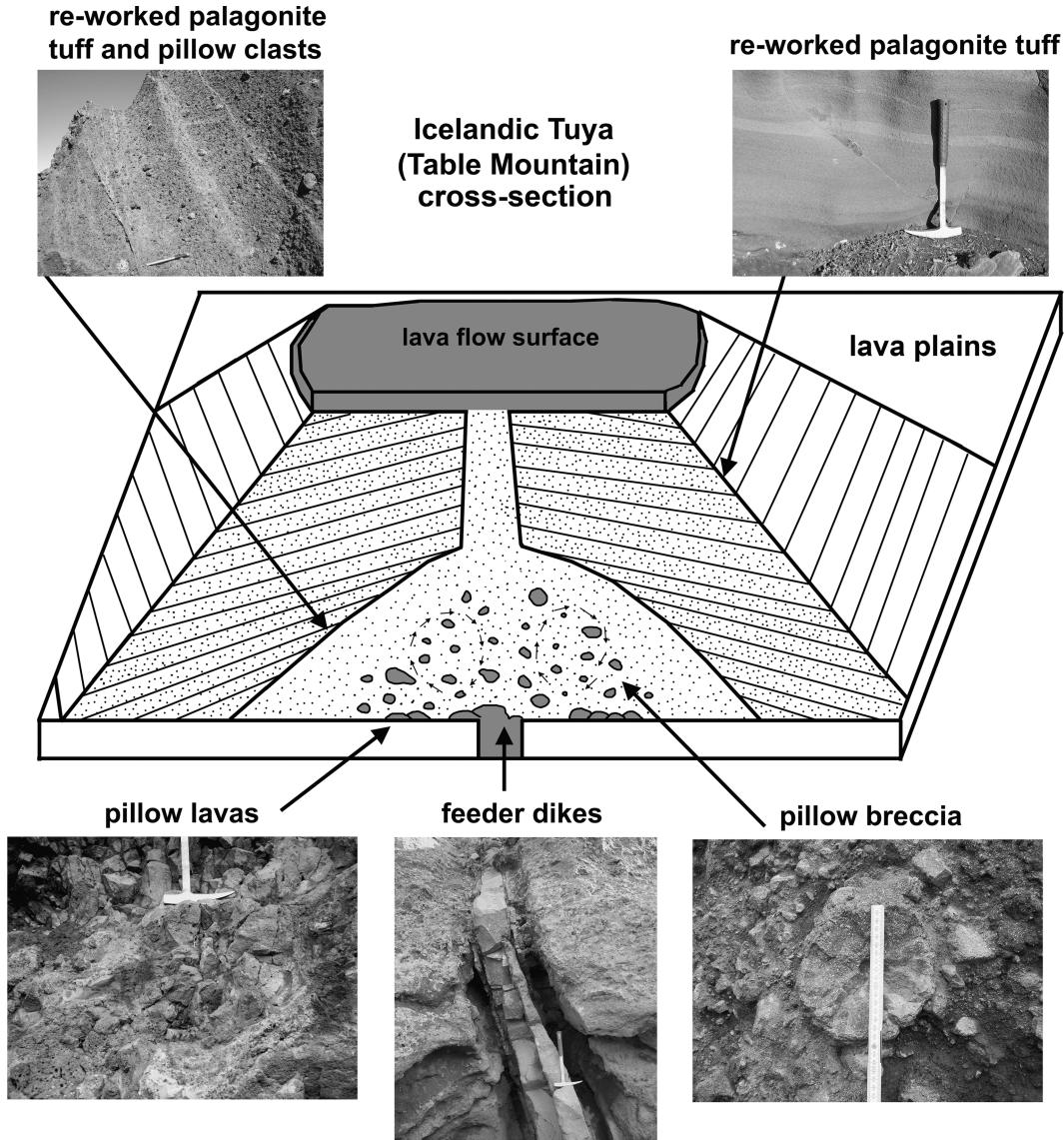

FIG. 16. Schematic of an Icelandic table mountain (tuya) showing general stratigraphy with accompanying photos. The basal sequence of a typical table mountain is dominated by pillow lavas and breccias showing evidence for secondary authigenic mineralization (zeolites, silica, clays). The mineral assemblage identified in this analysis within palagonite breccias from the Hlöðufell table mountain indicates mineralization at temperatures between 100°C and 140°C. By contrast, palagonite tuffs in the upper sequence of the table mountain show little evidence for advanced mineralization. Thin sections acquired from palagonitized tuffs reveal only thin Fe-oxide alteration rims around fresh, unaltered glass and limited authigenic mineralization in void spaces and fractures. Palagonite breccia and tuff samples collected from the sandur plains show similar variability in mineral characteristics and textures to the Hlöðufell samples, suggesting similar conditions of palagonite formation.

photographs from a series of Pleistocene-age table mountains located in the interior of Iceland near, and including, the Hlöðufell tuya. In the model illustrated, palagonite breccias were formed during the early stages of a subglacial eruption, when pillow lavas were intermixed with explosively fragmented basaltic glass (Fig. 16). Rapid hydrothermal alteration of volcanic glass occurred within the palagonitized breccia zone where glacial water circulated between high-temperature basal pillow lavas and the overlying, lower-temperature zone where volcanic breccias accumulated (Allen, 1980). The time required for palagonitization in basaltic phreatomagmatic systems was directly observed for volcanic tephras produced during the 1963 subaerial eruption at Surtsey (Jakobsson, 1978). Tephra from Surtsey underwent complete palagonitization within 3 years of the eruption. Even shorter timescales may be expected for basalt alteration within the basal sequences of subglacial volcanic systems, where high temperatures and high water-rock ratios coexist (*e.g.*, within pillow lava/breccia zones of tuyas).

As a subglacial volcanic edifice builds upward beneath a glacier, pressure reduction results in a transition from pillow basalt production to explosive fragmentation (Allen, 1980). Fine-grained, palagonitized hyaloclastites form in the upper region of the subglacial edifice (Fig. 16). If the volcanic edifice breaches the surface of the glacier, effusive volcanic activity will dominate, which thus allows for the eruption of sequence-capping lava flows.

X-ray powder diffraction analysis of the palagonite breccias that were collected from outcrops exposed in gullies on the south side of Hlöðufell table mountain revealed abundant secondary authigenic zeolites that include laumontite and analcime, similar to breccia clasts collected on the sandurs of southern Iceland (Fig. 7d). Petrographic thin sections of palagonitic breccias from Hlöðufell show vein and vesicle fills that contain zoned zeolites, with varying Na and Ca abundances (Fig. 8). The importance of authigenic zeolite formation in the palagonitization process is apparent in both the palagonite breccia samples collected from Hlöðufell and in the surface samples collected from the sandur plains of southern Iceland. Observations of zeolites in subglacial environments on Earth compare well with recent suggestions that zeolites may also be an important indicator of basalt/water interaction on Mars (Cloutis *et al.*, 2000; Ehlmann *et al.*, 2008).

In contrast, XRD analyses of palagonite tuffs collected from Hlöðufell, up section and distal to the palagonite breccia zone, produced no evidence for clays and zeolites, or other crystalline phases (Fig. 7d). Thin sections taken of these palagonitic tuffs reveal only thin Fe-oxide coatings formed during low-temperature palagonitization (Thorseth *et al.,* 1991; Bishop *et al.,* 2002) (Fig. 8). From these results, we suggest that the formation of secondary authigenic clays and zeolites was restricted to zones of palagonitization where breccias were in close contact with insulated pillow lavas. The mineral assemblage of the breccia clasts from Hlöðufell is suggestive of low-temperature (100–140°C) hydrothermal alteration (Fig. 17; Griffith and Shock, 1995).

For comparison to the tuya example, the results of the X-ray powder diffraction and spectral analysis of palagonitic breccias and coatings collected from the sandur plains reveal a similar mineral assemblage to the breccias collected at
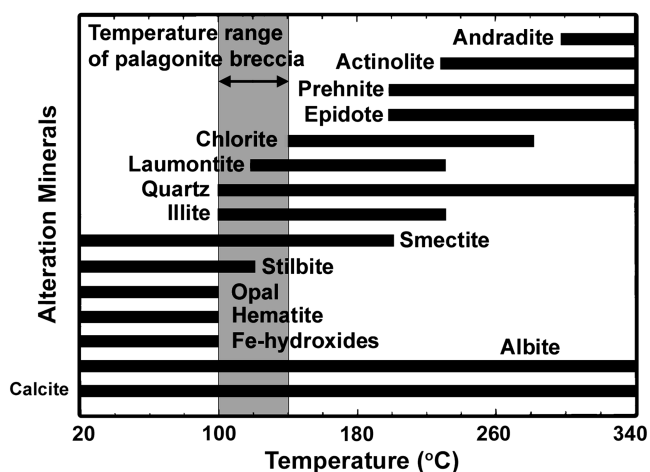

FIG. 17. Schematic of common minerals and their crystallization temperatures associated with Icelandic hydrothermal systems after Griffith and Shock (1995). The mineral assemblage of smectites, mixed-layer smectites and illite, zeolites, and low-temperature quartz, identified within palagonite breccias at the sandur plains and Hlöðufell, is consistent with crystallization temperatures between 100°C and 140°C, corresponding with the upper temperature range of habitability for microbial life.

Hlöðufell. Spectroscopic and XRD data suggest that the major smectite phase within the palagonites is nontronite. Di-octahedral (nontronite) and tri-octahedral (saponite) smectites dominate over an alteration temperature range of 0–100°C (Griffith and Shock, 1995). The identification of randomly ordered ($R < 1$) smectite/illite at 30–40% illite composition in the XRD clay analysis indicates an alteration temperature near 100°C (Moore and Reynolds, 1997). Randomly ordered smectite/illite is replaced by ordered ($R = 1$, 50–70% illite) smectite/illite at 120–180°C. Above 180°C smectite/illite mixed layered clays are dominated by illite, at concentrations $> 70\%$ (Mas *et al.*, 2003).

The identification of Na-Ca zeolites (heulandite, analcime, laumontite) in the clay analyses, as well as random bulk powder analyses, supports a temperature range of 100–170°C (Griffith and Shock, 1995; Robinson and Santana de Zamora, 1999). Low-quartz was identified both in hand samples of the sand-sized matrix component of sandur sediments and in the XRD analyses of the palagonitic materials (Fig. 7). At temperatures > 100°C, quartz is favored as the stable silica phase over opal-C and opal-CT (Griffith and Shock, 1995). Quartz has been identified, along with randomly ordered smectite/illite in the propylitic zone of rhyolitic hydrothermal systems (Ylagen *et al.,* 1996). The presence of crystalline quartz in a dominantly basaltic system is suggestive of a hydrothermal origin.

Remote identification of VNIR-SWIR absorption bands that are indicative of hydrated minerals on the sandur plains is consistent with ground truth evidence for low abundances of hydrothermally formed hydrated minerals in palagonite breccia clasts and coatings. Figures 6 and 13 illustrate the correlation between surface-mapped palagonite abundance and pixels identified in the remote analysis that exhibit Al-OH$^-$ and Si-OH$^-$ absorption features. This strong correlation suggests that the ASTER data can be used to identify

hydrated alteration materials on a dominantly dark basaltic surface. Lab spectroscopic data show that, for the sand-sized sandur mixture samples, the palagonite absorption features are masked where dark unaltered basaltic clasts dominate (Fig. 9). In intimate mixtures, like the sandur sand mixtures, dark clasts absorb most of the light that falls on the surface, which allows less light to penetrate the sample. In fine-grained dark samples with a low abundance of light materials, this effect may completely mask the absorptions from the lighter clasts (Clark, 1999; Milliken and Mustard, 2007). Lab spectral analyses of sandur mixtures having palagonite abundances <5% showed that the absorption features typical of (but not unique to) the palagonitized materials at $1.0 \mu m$ (Fe^{3+}), $1.4 \mu m$ (OH^-), $1.9 \mu m$ (H_2O and OH^-), and 2.2–2.3 μm (Fe, Mg, Al, $Si-OH^-$) are largely absent or are unobservable above the instrument noise (Figs. 9 and 10). At $\sim 20\%$ abundance these absorption features are obvious. As the Iceland case proves, this nonlinear, intimate mixing is a complicating factor in the identification of light-toned minerals (like palagonite) that may occur at small abundances in fine-grained surface sediments on Mars (Milliken and Mustard, 2007).

Furthermore, our study suggests that remote identification of palagonite on a dark surface is likely to be more effective where the particle sizes are coarse (cobble to boulder). For boulder-sized surfaces, the physics of intimate mixing is replaced by patchwork mixing, where light particles dominate the spectra (Clark, 1999). Therefore, the mapped high abundance of alteration in the proximal zone of Skeiðarársandur, which was obtained from ASTER data, may in part reflect particle size effects, as this region is characterized by not only a higher abundance of palagonite but also of longitudinal bars comprised of cobbles and boulders. As demonstrated for Mýrdalssandur, few variations in the spatial distribution of palagonite were observed on the ground or with the ASTER remote sensing data. This may be related to a compositional homogeneity of the surface at Mýrdalssandur or a textural difference relative to Skeiðarársandur. The surface of Mýrdalssandur is dominated by sand-granule-sized juvenile pumice clasts with boulder fields on the lee side of proximal, isolated bedrock remnants. However, on the 1918 flood surface, in the immediate pro-glacial zone, the well-sorted boulder and cobble fields that characterize the 1996 flood surface of proximal Skeiðarársandur are less extensive.

5.2. Implications for detectability on Mars

The remote and lab identification of palagonite in Icelandic sandur materials holds important implications for Mars. The presence of distinctive mineral assemblages on sandur surfaces suggests hydrothermal conditions between 100°C and 140°C, and provides a mineralogical fingerprint for potentially habitable environments beneath Icelandic glaciers that overlap the known upper temperature limit for hyperthermophilic extremophiles (Kashefi and Lovley, 2003). The future identification of similar palagonitized materials on Mars, in association with geomorphic and sedimentological features of probable fluvial origin or volcanic origin, or both, may provide evidence for past or present, low-temperature hydrothermal environments. Such environments have been assigned as high-priority sites for future

astrobiology missions to Mars (Walter and Des Marais, 1993; Farmer, 1996, 2000).

Several previous studies have analyzed weathered and hydrothermally altered basalts and tephras in terrestrial settings and described the alteration textures, chemistry, and mineralogies (e.g., Allen et al., 1981; Thorseth et al., 1991; Bishop et al., 2002; Drief and Schiffman, 2004; Nelson et al., 2005; Pokrovsky et al., 2005; Bishop et al., 2007; Hamilton et al., 2008). In confirmation of this previous work, our study has shown that mineralogical differences are apparent in the X-ray diffractograms of palagonite tuffs and palagonite breccias that formed under vastly different temperature, pressure, and water/rock regimes within subglacial settings (Fig. 7). Increased crystallinity and the presence of authigenic phases in the samples are apparent indicators of the degree of alteration and may be used in future spectral and ground-based analyses of specific hydrated units on Mars to distinguish alteration conditions.

However, difficulty in the remote identification of palagonite on Mars lies in its heterogeneous mineralogy that, in many cases, is genetically non-unique. For the Iceland case, where field observations are possible, hydrated mineral signatures associated with clays, zeolites, and other silicates can be tied directly to palagonitic materials and subglacial hydrothermal environments. However, the remote identification of similar minerals on Mars requires the possibility for a broad range of possible aqueous alteration environments, and each interpretation of the conditions of alteration holds major implications regarding the planet's geological and climatic history. As an example, the results of our study have shown that the identification of specific zeolites on Mars (e.g., laumontite) could be an important, though non-unique, indicator for low-temperature (100–140°C) hydrothermal palagonitization of basaltic crust. Putative zeolites associated with smectite-bearing materials have been detected in CRISM data for deltaic deposits within Jezero Crater in the southern highlands of Mars (Ehlmann et al., 2008) and are candidate compositional analogues for the Icelandic example presented here.

A complicating factor in the identification of hydrated phases at specific locations on Mars is the likelihood of mineralogical and lithologic mixtures. Results of the clay analysis of palagonite clasts and coatings presented in this study reveal specific ordering conditions for smectite-illite mixtures that can be used to infer the temperature of crystallization. Such an analysis is, however, currently unavailable for Mars. As another example, the lab VNIR-SWIR spectrum of an isolated zeolite (heulandites) in Fig. 11 is similar, within the spectral range of 0.35–2.5 μm, to the lab spectrum for a heterogeneous palagonite breccia clast containing both smectite minerals and secondary zeolite vein fills (Fig. 9). Absorptions at 1.4, 1.9, and 2.2–2.3 μm are common to heterogeneous palagonite clasts, zeolites, and pure phase clays. Broadening of the OH^-/H_2O absorptions in the palagonite samples, relative to the features in the pure-phase zeolite samples (Figs. 9 and 11), may be an important indicator of the overlap of absorption bands in clay-zeolite mixtures. Specifically, for zeolites, the shape of the OH^-/H_2O absorption at 1.4 μm is a distinctive feature (Cloutis et al., 2000) but is influenced by the occurrence of the 1.4 μm absorption associated with clay minerals. Furthermore, for remote identification, interference with atmospheric water

makes the identification of the 1.4 μm feature on Earth and Mars difficult. These observations suggest that definitive identification of palagonites and pure phase zeolites/clays on Mars may be difficult with remote spectrometers of low spectral resolution. Use of multiple diagnostic remote sensing and ground-based tools to distinguish pure mineral phases from mixtures is therefore required.

5.3. Implications for previous identifications on Mars

Previous interpretations of the formation environment of hydrated mineral-bearing units on Mars are challenged by the difficulty in the identification of pure-phase minerals within mineralogical mixtures, heterogeneous lithologies, and clast mixtures. Often in the literature, clays identified on the Noachian-age highlands have been attributed to episodic aqueous weathering of basalt during an early warm-wet phase of martian history (*e.g.*, Poulet *et al.*, 2005; Bibring *et al.*, 2006; Tosca and Knoll, 2009). This has led to the creation of a new mineralogical timescale for Mars, where the Phyllocian epoch defines the early period of potentially Earth-like climate conditions (Bibring *et al.*, 2006). Although this conclusion is consistent with the overall broad distribution of clays across Noachian-age surfaces, the interpretations are limited by the assumption that the spectral features are unique to a pure-phase clay, given the current spectral resolution of orbiting VNIR-SWIR spectrometers. Alternatively, some of the clay observations may be the result of hydro-

thermal alteration of the martian crust during Noachian-age volcanic or impact events (Newsom, 1980; Ehlmann *et al.*, 2008). Although deposits formed by these mechanisms are likely to be isolated at specific locations on the martian surface (Mustard *et al.*, 2008), reworking of these mineralogically similar materials by wind or water may have increased their total area of distribution.

As an example clay observation on Mars, Fig. 18 from Poulet *et al.* (2005) shows an OMEGA spectrum collected from a "dark" unit at Syrtis Major. This spectrum contains absorption features at 1.9 and 2.29 μm, which were suggested by these authors to be most consistent with nontronite, a common secondary component of intense or long-term aqueous basalt alteration under Earth-like weathering conditions (*e.g.*, Allen *et al.*, 1981; Griffith and Shock, 1995; Bishop *et al.*, 2002). Our analysis of Icelandic sandurs indicated that similar absorptions at 1.9 and 2.29 μm are also common to palagonitic breccias and coatings that contain a heterogeneous mixture of Fe/Mg-rich clays, Fe oxides, zeolites, and silica, formed under low-temperature hydrothermal conditions. Furthermore, the example Syrtis Major spectrum has a significantly lower absolute reflectance compared to the presented lab spectra of the pure-phase clay (Fig. 18). From our observations of sandur clast mixtures, one possible explanation for this low absolute reflectance is the presence of an intimate mixture of dark, energy-absorbing clasts with a low abundance of lighter, clay-rich material. Alternatively, because the overall reflectance decreases as the grain size increases (Clark, 1999), the low absolute reflectance of the Syrtis Major spectra may be due to the presence of bedrock or large boulder-sized clasts. However, Syrtis Major is a basaltic volcanic system (Hiesinger and Head, 2004; Mustard *et al.*, 2007), and the identified dark materials are likely a bedrock or wind-blown component of unaltered basalt. In our analysis of the Icelandic sandur plains, minor abundances (>5%) of light-toned palagonite were detected from orbit and in the lab despite the presence of a dark basaltic matrix. In addition, an unquantifiable abundance of some unaltered basaltic clasts at both sandurs exhibited palagonite coatings and amygdules of zeolites and clays that may have served to increase the overall reflectance of the sandur surface. On the sandurs, palagonite coatings on unweathered basaltic clasts were likely derived from clay-rich water that percolated through the porous volcanic sediment during the waning stages of a jökulhlaup. Similar coatings could be common on altered basaltic clasts in hydrothermal or fluvial environments on Mars.

Similar to the Syrtis Major observation, phyllosilicate-rich units were identified in Nili Fossae by Poulet *et al.* (2008), who used OMEGA data, and Mustard *et al.* (2008), who used CRISM. The Nili Fossae deposit spans a region of 10^6 km^2 within ancient, heavily cratered Noachian-age terrain and may have formed by the low-temperature aqueous alteration of basaltic materials in a fluvial-lacustrine system (Mangold *et al.*, 2007; Ehlmann *et al.*, 2008; Mustard *et al.*, 2008). Poulet *et al.* (2008) used a radiative transfer model applied to OMEGA spectral data to demonstrate that the deposits within the Nili Fossae layered units contain only minor fractions of altered material surrounded by unaltered mafic material, similar to our Iceland case. Additionally, CRISM observations of the Nili Fossae deposit (Mustard *et al.*, 2008) identified smectites in close association with olivine-bearing
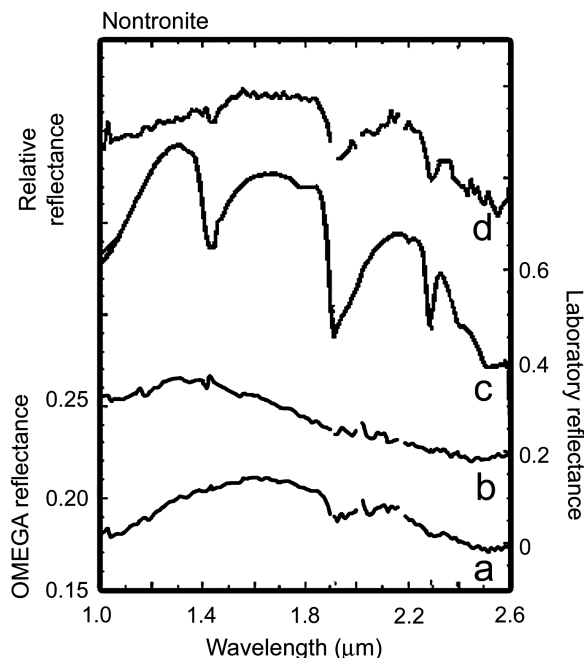

FIG. 18. OMEGA and lab spectra of nontronite, from Poulet *et al.* (2005). (**a**) An atmospherically corrected OMEGA spectrum from Nili Syrtis Mensae displaying an absorption feature at 2.29 μm suggested to represent the pure phase of nontronite. Also note the shallow 1.4 μm absorption feature and the deep 1.9 μm feature that is suggestive of H₂O and OH⁻ bound minerals. (**b**) Atmospherically corrected Mars reference spectrum. (**c**) Laboratory spectra of nontronite. (**d**) Spectral ratio of (a) and (b).

bedrock. The interpretation of *in situ* weathering for the origin of these clay-bearing units therefore seems unlikely, given the intimate association of altered and unaltered mafic material. A possible likely hypothesis for this observation is that the Nili Fossae layered deposits were transported from a compositionally heterogeneous source region that contained both clays and unaltered mafics. The possibility of a hydrothermal source region for these deposits can therefore not be entirely ruled out.

5.4. Possible Icelandic analog sites on Mars

Clifford (1987) and Carr (1996) suggested that a global groundwater system is present on Mars at a depth of several kilometers below the surface. In addition, geothermal melting of the martian cryosphere may have provided sustained subsurface hydrothermal environments for the evolution and persistence of thermophilic life (Gulick, 1998; Farmer, 2003). Deep drilling appears to be beyond current robotic technologies for the exploration of Mars. However, natural geological processes, such as hydrothermal upwelling or catastrophic floods, could bring groundwater and hydrothermal deposits from the deep subsurface hydrosphere (along with any putative life-forms present) to the surface where it could be more easily sampled (Farmer, 2002). While variations in the depth and thickness of the global cryosphere are unknown, the Gamma Ray Spectrometer on board Mars Odyssey has detected abundant near-surface ice within the upper half meter of the regolith, at latitudes >60° (Mitrofanov *et al.,* 2003; Boynton *et al.,* 2006). It seems likely that wherever shallow magmatic intrusions have come into contact with the martian cryosphere, or with groundwater, hydrothermal systems would have developed. Identification of fluvial sediments derived from these interactions and containing hydrothermally altered materials may point to primary locations of hydrothermal activity. On Earth, the venting of upwelling hydrothermal waters at the surface produces characteristic geomorphic features (small mounds and channel networks) and sinter deposits dominated by characteristic hydrothermal mineral assemblages. The mineralization processes at springs and within rivers or streams that commonly accompany shallow hydrothermal systems can provide especially favorable conditions for the capture and preservation of fossil biosignatures (Walter and Des Marais, 1993; Cady and Farmer; 1996; Farmer, 2000, 2003; Meyer-Dombard *et al.,* 2007). Interest in hydrothermal environments as exploration targets for past martian life has increased with recent discoveries of geomorphic features (Allen and Oehler, 2008) and mineralogical associations of probable hydrothermal origin (Squyres *et al.,* 2008) on Mars.

The primary evidence for a deep (1–2 km) subsurface global hydrosphere/cryosphere in the past on Mars is the Hesperian to Early Amazonian-age catastrophic outflow channels. These immense channels are sourced within the southern highland terrains and empty into the northern lowlands (Carr, 1979; Baker *et al.,* 1991; Rotto and Tanaka, 1995; Tanaka, 1997; Marchenko *et al.,* 1998; Nelson and Greeley, 1999; Burr *et al.,* 2002). The midlatitude catastrophic outflow channels extend several hundred kilometers from source regions that are marked by "chaos" terrains. These chaos terrains are likely collapse features, formed from catastrophic water release as the deep hydrosphere became

pressurized by the overburden of a thickened cryosphere (Carr, 1987). Geomorphic features associated with some chaos terrains (*e.g.,* Aram Chaos, Iani Chaos) have been shown to contain mineral signatures (*e.g.,* specular hematite deposits) indicative of ancient aqueous or possibly hydrothermal activity (Glotch and Christensen, 2005; Glotch and Rogers, 2007; Massé *et al.,* 2008).

The catastrophic release of liquid water at some locations has been directly linked to geothermal melting of the martian cryosphere (McKenzie and Nimmo, 1999). Putative volcanic landforms have been shown to be associated with the headreaches of some outflow channels, including volcanic vents within Melas Chasma (Chapman and Lucchitta, 2000), volcanic cones and exposed igneous intrusions at Aram Chaos (Lanz and Jaurnann, 2001), possible phreatomagmatic deposits and cones at Hrad Vallis (Wilson and Mouginis-Mark, 2003b; Morris and Mouginis-Mark, 2006), dike swarms at the head of Athabasca Vallis (Burr *et al.,* 2002), pyroclastic flow deposits at Mangala Valles (Wilson and Head, 2004), and volcanic-like conical landforms at Hydraotes Chaos (Meresse *et al.,* 2008). These regions represent ideal sites for astrobiological exploration and the identification of martian palagonite, particularly in light of recent remote identifications of hydrated minerals at some of these locations (Glotch and Christensen, 2005; Massé *et al.,* 2008). However, in many cases, identifications of hydrated minerals within outflow channels are limited to Noachian-age exposures along the canyon walls and are not associated with specific flood deposits (*e.g.,* McKeown *et al.,* 2009). These units may represent ancient reworked hydrothermal deposits or weathered basalts and cannot currently be directly linked as geomorphological and mineralogical analogues to the Icelandic sandur plains.

Evidence for more recent localized overland water flow is found in the form of small valley networks at high elevations on several Hesperian to Amazonian-age volcanoes in the Tharsis, Elysium, and Hellas regions (*e.g.,* Gulick, 1998; Dohm *et al.,* 2004; Fassett and Head, 2007). Channel networks located on the flanks of Hadriaca Patera, Tyrrhena Patera, and Apollonius Patera have been attributed to pyroclastic flow or releases of hydrothermal fluids (Farmer, 1996; Gregg *et al.,* 2002; Farmer, 2004; Williams *et al.,* 2008). These systems, although several orders of magnitude smaller in dimension than the midlatitude catastrophic outflow channels, may also provide confirming mineralogical evidence for ancient habitable environments in the subsurface, sustained by hydrothermal processes.

Finally, large chasmata at the north and south poles of Mars, including Chasma Boreale in the north and Chasma Australe in the south, have been suggested to originate from fluvial erosion during catastrophic releases of subglacial liquid water reservoirs formed by basal melting from ice overburden or subglacial volcanic eruptions (Clifford, 1980, 1987; Benito *et al.,* 1997; Anguita *et al.,* 2000; Fishbaugh and Head, 2002), although this hypothesis is controversial owing to the strong evidence for aeolian/solar ablation origin mechanisms (Howard, 1980; Warner and Farmer, 2008a, 2008b). Large, arcuate depressions present at the heads of the chasmata are postulated to have formed by sudden meltwater releases, followed by the collapse of overlying ice-rich polar layered deposits. These putative subcap liquid water environments on Mars have been compared on Earth to

subglacial lake systems that occur in Antarctica and Iceland. Such environments may have also been ideal locations for the development of martian hydrothermal systems capable of supporting thermophilic, subsurface chemotrophic microbes.

6. Conclusion

Icelandic sandur plains exhibit specific geomorphological, sedimentological, and compositional features that are conditioned by periodic catastrophic outfloods from subglacial environments. In these environments, hydrothermal processes have altered basaltic volcanic materials and produced a variety of low-temperature hydrothermal mineral assemblages. Catastrophic outfloods that result from magma/ice interactions hold great importance for astrobiology as a mechanism for delivering important information about subsurface habitable environments on Mars to surface environments where important mineralogical information may be detected by either orbital remote sensing or ground-based methods of exploration.

The results of this analysis indicate that palagonite, altered within a low-temperature (100–140°C) hydrothermal subglacial environment and found within associated outflood deposits, may be an important surface indicator for past habitable hydrothermal environments on Mars. However, our results also demonstrate the complexity in confirming both the existence and the origin of palagonite within martian deposits given (1) its heterogeneous texture and mineralogy, (2) the non-unique mechanism of formation for specific minerals associated with palagonite (*e.g.*, nontronite clay), (3) its possible occurrence in low abundances within fine-grained mixtures of dark, energy-absorbing unaltered basaltic material, and (4) the lack of indisputable morphological evidence on Mars for fluvial sediments and channels associated with magma/ice interaction.

Despite these uncertainties, this study provides a lithologic and genetic end member for future interpretations of the origin of specific hydrated mineral assemblages on Mars. Terrestrial analogue studies such as these enable more informed comparisons to Mars and help to identify the most favorable landing sites to explore for past or present habitable environments and life. Many studies have shown that similar hydrothermal environments on Earth capture and preserve a broad range of fossil biosignatures and are therefore highly regarded as targets for future life-detection missions (Walter and Des Marais, 1993; Farmer, 1998, 2000; Hofmann and Farmer, 2000). This study shows that the proglacial fluvial environments that are associated with subglacial volcanism in Iceland contain detectable mineral signatures of low-temperature hydrothermal activity within the temperature range of terrestrial life. Current and future high-resolution image and spectral analyses of the floors of martian catastrophic outflow channels may reveal specific sedimentological, stratigraphic, and compositional features indicative of subsurface magma/ice interaction. In addition, smaller-scale fluvial valley systems within periglacial settings should also be given a high priority for future orbital mapping efforts. In particular, future efforts should continue to emphasize the search for unique hydrated mineral assemblages that commonly form during the hydrothermal alteration of basaltic material.

Author Disclosure Statement

No competing financial interests exist.

Abbreviations

ASTER, Advanced Spaceborne Thermal Emission and Reflection Radiometer; CRISM, Compact Reconnaissance Imaging Spectrometer; MNF, Minimum Noise Fraction Transformation; MTMF, Mixed Tuned Matched Filtering; PPI, Pixel Purity Index; SAM, Spectral Angle Mapper; SWIR, shortwave infrared; USGS, United States Geological Survey; VNIR, visible light–near infrared; XRD, X-ray diffraction.

References

Allen, C.C. (1980) Icelandic sub-glacial volcanism: thermal and physical studies. *Geology* 88:108–117.

Allen, C.C. and Oehler, D.Z. (2008) A case for ancient springs in Arabia Terra, Mars. *Astrobiology* 8:1093–1112.

Allen, C.C., Gooding, J.L., Jercinovic, M., and Keil, K. (1981) Altered basaltic glass: a terrestrial analog to the soil of Mars. *Icarus* 45:347–369.

Anguita, F., Babin, R., Benito, G., Gomez, D., Collado, A., and Rice, J. (2000) Chasma Australe, Mars: structural framework for a catastrophic outflow origin. *Icarus* 144:302–312.

Arnórsson, S. (1975) Application of the silica geothermometer in low temperature hydrothermal areas in Iceland. *Am. J. Sci.* 275:763–784.

Arnórsson, S., Gunnlaugsson, E., and Svavarsson, H. (1983) The chemistry of geothermal waters in Iceland; III, Chemical geothermometry in geothermal investigations. *Geochim. Cosmochim. Acta* 47:567–577.

Baker, V.R., Strom, R.G., Gulick, V.C., Kargel, J.S., and Komatsu., G. (1991) Ancient oceans, ice sheets and the hydrological cycle on Mars. *Nature* 352:463–464.

Benito, G., Mediavilla, F., Fernandez, M., Marquez, A., Martinez, J., and Anguita. F. (1997) Chasma Boreale, Mars: a sapping outflow channel with a tectono-thermal origin. *Icarus* 129:528–538.

Bibring, J.P., Langevin, Y., Mustard, J.F., Poulet, F., Arvidson, R., Gendrin, A., Gondet, B., Mangold, N., Pinet, P., Forget, F., and the OMEGA Team. (2006) Global mineralogical and aqueous Mars history derived from OMEGA/Mars Express data. *Science* 312:400–404.

Bishop, J.L. and Pieters, C.M. (1995) Low-temperature and low atmospheric pressure infrared reflectance spectroscopy of Mars soil analog materials. *J. Geophys. Res.* 100:5369–5379.

Bishop, J.L., Schiffman, P., and Southard, R. (2002) Geochemical and mineralogical analyses of palagonitic tuffs and altered rinds of pillow basalts in Iceland and applications to Mars. In *Volcano-Ice Interaction on Earth and Mars,* Geological Society of London Special Publication 202, pp 371–392.

Bishop, J.L., Schiffman, P., Murad, E., Dyar, M.D., Drief, A., and Lane, M.D. (2007) Characterization of alteration products in tephra from Haleakala, Maui: a visible-infrared spectroscopy, Mossbauer spectroscopy, XRD, EMPA and TEM study. *Clays Clay Miner.* 55:1–17.

Bishop, J.L., Lane, M.D., Dyar, M.D., Parente, M., Roach, L.H., Murchie, S.L., and Mustard, J.F. (2008) Sulfates on Mars: how recent discoveries from CRISM, OMEGA and the MERs are changing our view of the planet. *Geochim. Cosmochim. Acta* 72:A86.

Boynton, W.V., Reedy, R.C., and Taylor, G.J. (2006) Elemental maps of Mars from the Mars Odyssey gamma-ray spectrometer. *Meteorit. Planet. Sci.* 41:A27.

Burr, D.M., McEwen, A.S., and Sakimoto, S.E.H. (2002) Recent aqueous floods from the Cerberus Fossae, Mars. *Geophys. Res. Lett.* 29, doi:10.1029/2001GL013345.

Cady, S.L. and Farmer, J.D. (1996) Fossilization processes in siliceous thermal springs: trends in preservation along thermal gradients. In *Evolution of Hydrothermal Ecosystems on Earth (and Mars?), Ciba Foundation Symposium 202,* edited by G.R. Bock and J.A. Goode, John Wiley and Sons, Chichester, UK, pp 150–173.

Carr, M.H. (1979) Formation of martian flood features by release of water from confined aquifers. *J. Geophys. Res.* 84:2995–3007.

Carr, M.H. (1987) Water on Mars. *Nature* 326:30–35.

Carr, M.H. (1996) Channels and valleys on Mars: cold climate features formed as a result of a thickening cryosphere. *Planet. Space Sci.* 44:1411–1423.

Chapman, M.G. and Lucchitta, B.K. (2000) New Mars data suggest Melas Chasma interior deposits are sub-ice volcanoes. In *Abstracts with Programs,* Vol. 32, Geological Society of America, Boulder, CO, p 304.

Chapman, M.G. and Tanaka, K.L. (2002) Related magma-ice interactions: possible origins of chasmata, chaos, and surface materials in Xanthe, Margaritifer, and Meridiani Terrae, Mars. *Icarus* 155:324–339.

Chapman, M.G., Gudmundsson, M.T., Russell, A.J., and Hare, T.M. (2003) Possible Juventae Chasma subice volcanic eruptions and Maja Valles ice outburst floods on Mars: implications of Mars Global Surveyor crater densities, geomorphology, and topography. *J. Geophys. Res.* 108, doi:10.1029/2002JE002009.

Christensen, P.R., Bandfield, J.L., Hamilton, V.E., Ruff, S.W., Kieffer, H.H., Titus, T.N., Malin, M.C., Morris, R.V., Lane, M.D., Clark, R.L., Jakosky, B.M., Mellon, M.T., Pearl, J.C., Conrath, B.J., Smith, M.D., Clancy, R.T., Kuzmin, R.O., Roush, T., Mehall, G.L., Gorelick, N., Bender, K., Murray, K., Dason, S., Greene, E., Silverman, S., and Greenfield, M. (2001) Mars Global Surveyor Thermal Emission Spectrometer experiment: investigation description and surface science results. *J. Geophys. Res.* 106:23823–23871.

Christensen, P.R., Ruff, S.W., Fergason, R., Gorelick, N., Jakosky, B.M., Lane, M.D., McEwen, A.S., McSween, H.Y., Mehall, G.L., Milam, K., Moersch, J.E., Pelkey, S.M., Rogers, A.D., and Wyatt, M.B. (2005) Mars Exploration Rover candidate landing sites as viewed by THEMIS. *Icarus* 176:12–43.

Clark, R. (1999) Spectroscopy of rocks and minerals, and principles of spectroscopy. In *Remote Sensing for the Earth Sciences,* Manual of Remote Sensing, Vol. 3, edited by A.N. Rencz, John Wiley and Sons, New York, pp 3–58.

Clark, R.N., King, T.V., Klejwa, M., and Swayze, G.A. (1990) High spectral resolution reflectance spectroscopy of minerals. *J. Geophys. Res.* 95:12653–12680.

Clifford, S. (1980) (85°N, 0°W): Remnant of a martian jökulhlaup? *Bulletin of the American Astronomical Society* 12:678.

Clifford, S. (1987) Polar basal melting on Mars. *J. Geophys. Res.* 92:9135–9152.

Cloutis, E.A., Asher, P.M., Mertzman, S.A., and Guertin, M. (2000) Spectral-compositional properties of zeolites [abstract 1172]. In *Proceedings of the 31st Lunar and Planetary Science Conference,* Lunar and Planetary Institute, Houston.

Crisp, J.A. and Bartholomew, M.J. (1992) Mid-infrared spectroscopy of Pahala ash palagonite and implications for remote sensing studies of Mars. *J. Geophys. Res.* 97:14691–14699.

Dohm, J.M., Ferris, J.C., Barlow, N.G., Baker, V.R., Mahaney, W.C., Anderson, R.C., and Hare, T.M. (2004) The northwestern slope valleys (NSVs) region, Mars: a prime candidate site for the future exploration of Mars. *Planet. Space Sci.* 52:189–198.

Drief, A. and Schiffman, P. (2004) Very low-temperature alteration of sideromelane in hyaloclastites and hyalotuffs from Kilauea and Mauna Kea volcanoes: implications for the mechanism of palagonite formation. *Clays Clay Miner.* 52:622–634.

Duller, R.A., Mountney, N.P., Russell, A.J., and Cassidy, N.C. (2008) Architectural analysis of a volcanoclastic jökulhlaup deposit, southern Iceland: sedimentary evidence for supercritical flow. *Sedimentology* 55, doi:10.1111/j.1365–3091.2007.00931.x.

Eberl, D.D. (2003) User's guide to RockJock—a program for determining quantitative mineralogy from powder X-ray diffraction. U.S. Geological Survey Open-File Report 03-78, U.S. Geological Survey, Boulder, CO.

Ehlmann, B.L., Mustard, J.F., Fassett, C., Schon, S.C., Head, J.W., Des Marais, D.J., Grant, J.A., and Murchie, S.L. (2008) Clay minerals in delta deposits and organic preservation potential on Mars. *Nat. Geosci.* 1:355–358.

Farmer, J.D. (1996) Hydrothermal systems on Mars: an assessment of present evidence. In *Evolution of Hydrothermal Ecosystems on Earth (and Mars?), Ciba Foundation Symposium 202,* edited by G.R. Bock and J.A. Goode, John Wiley and Sons, Chichester, UK, pp 273–299.

Farmer, J.D. (1998) Thermophiles, early biosphere evolution and the origin of life on Earth: implications for the exobiological exploration of Mars. *J. Geophys. Res.* 103:28457–28461.

Farmer, J.D. (2000) Hydrothermal systems: doorways to early biosphere evolution. *GSA Today* 10:1–9.

Farmer, J.D. (2002) Prospecting for modern and ancient hydrothermal systems on Mars: implications for astrobiology and the exploration for past or present life [abstract #P61D-07]. In *American Geophysical Union, Fall Meeting 2002,* American Geophysical Union, Washington DC.

Farmer, J.D. (2003) Exploring for a fossil record of extraterrestrial life. In *Palaeobiology II,* edited by D. Briggs and P.R. Crowther, Blackwell Science, Malden, MA, pp 8–13.

Farmer, J.D. (2004) Martian hydrothermal systems; targets in the exploration for extraterrestrial life [abstract 197-2]. In *32nd International Geological Congress,* Florence, Italy.

Farmer, J.D. and Des Marais, D.J. (1996) Hydrothermal deposits as targets for Mars exopaleontology. In *Abstracts with Pro-*

grams, Vol. 28, Geological Society of America, Boulder, CO, p 129.

Fassett, C.I. and Head, J.W. (2007) Valley formation on martian volcanoes in the Hesperian: evidence for melting of summit snowpack, caldera lake formation, drainage and erosion on Ceraunius Tholus. *Icarus* 189:118–135.

Fishbaugh, K.E. and Head, J.W. (2002) Chasma Boreale, Mars: topographic characterization from Mars Orbiter Laser Altimeter data and implications for mechanisms of formation. *J. Geophys. Res.* 107, doi:10.1029/2000JE001351.

Fujisada, H. (1995) Design and performance of ASTER instrument. *Proc. Soc. Photo. Opt. Instrum. Eng.* 2583:16–25.

Glotch, T.D. and Christensen, P.R. (2005) Geologic and mineralogic mapping of Aram Chaos: evidence for a water-rich history. *J. Geophys. Res.* 110, doi:10.1029/2004JE002389.

Glotch, T.D. and Rogers, A.D. (2007) Evidence for aqueous deposition of hematite- and sulfate-rich light-toned layered deposits in Aureum and Iani Chaos, Mars. *J. Geophys. Res.* 112, doi:10.1029/2006JE002863.

Gomez, B., Smith, L.C., Magilligan, F.J., Mertes, L.A.K., and Smith, N.D. (2000) Glacier outburst floods and outwash plain development: Skeiðarársandur, Iceland. *Terra Nova* 12:126–131.

Gregg, T.K.P., Crown, D.A., and Sakimoto, S.E.H. (2002) Between a rock and a hard place; Noachian highlands, Hesperian lowlands and Tyrrhena Patera. In *Abstracts with Programs,* Vol. 34, Geological Society of America, Boulder, CO, p 71.

Griffith, L.L. and Shock, E.L. (1995) A geochemical model for the formation of hydrothermal carbonates on Mars. *Nature* 377:406–408.

Gudmundsson, M.T. and Hognadottir, T. (2007) Volcanic systems and calderas in the Vatnajökull region, central Iceland: constraints on crustal structure from gravity data. *Journal of Geodynamics* 43:153–169.

Gudmundsson, M.T., Sigmundsson, F., and Bjornsson, H. (1997) Ice-volcano interaction of the 1996 Gjalp subglacial eruption, Vatnajokull, Iceland. *Nature* 389:954–957.

Gulick, V.C. (1998) Magmatic intrusions and a hydrothermal origin for fluvial valleys on Mars. *J. Geophys. Res.* 103:19365–19387.

Hamilton, V.E., Morris, R.V., Gruener, J.E., and Mertzman, S.A. (2008) Visible, near infrared, and middle infrared spectroscopy of altered basaltic tephras: spectral signatures of phyllosilicates, sulfates, and other aqueous alteration products with application to the mineralogy of the Columbia Hills of Gusev Crater, Mars. *J. Geophys. Res.* 113, doi:10.1029/2007JE003049.

Helgason, J. and Duncan, R.A. (2001) Glacial-interglacial history of the Skaftafell region, southeast Iceland, 0–5 Ma. *Geology* 29:179–182.

Hiesinger, H. and Head, J.W. (2004) The Syrtis Major volcanic province, Mars: synthesis from Mars Global Surveyor data. *J. Geophys. Res.* 109, doi:10.1029/2003JE002143.

Hofmann, B.A. and J.D. Farmer. (2000) Filamentous fabrics in low-temperature mineral assemblages: are they fossil biomarkers? Implications for the search for a subsurface fossil record on the early Earth and Mars. *Planet. Space Sci.* 48:1077–1086.

Howard, A. (1980) The effect of wind scarp evolution on the martian poles. NASA Technical Memorandum 82385, NASA, Washington DC, pp 333–335.

Hunt, G.R. (1977) Spectral signatures of particulate materials in the visible and near infrared. *Geophysics* 42:501–513.

Jakobsson, S.P. (1978) Environmental factors controlling the palagonitization of the Surtsey tephra, Iceland. *Bulletin of the Geological Society of Denmark* 27:91–105.

Jakobsson, S.P. and Moore, J.G. (1986) Hydrothermal minerals and alteration rates at Surtsey Volcano, Iceland. *Geol. Soc. Am. Bull.* 97:648–659.

Kashefi, K. and Lovley, D.R. (2003) Extending the upper temperature limit for life. *Science* 301:934.

Knudsen, Ó., Jóhannesson, H., Russell, A.J., and Haraldsson, H. (2001) Changes in the Gígjukvísl River channel during the November 1996 jökulhlaup, Skeiðarársandur, Iceland. *Jökull* 50:19–32.

Kraft, M.D., Sharp, T.G., Michalski, J.R., and Rampe, E.B. (2007) Basalt weathering at high-latitude regions on Mars. *Geochim. Cosmochim. Acta.* 71:A519.

Kristmannsdóttir, H. and Tómasson, J. (1978) Zeolite zones in geothermal areas in Iceland. In *Natural Zeolite Occurrence, Properties and Use,* edited by L.B. Sand and F.M. Mumpton, Pergamon Press, Oxford, pp 277–284.

Kruse, F.A., Lefkoff, A.B., Boardman, J.B., Heidebreicht, K.B., Shapiro, A.T., Barloon, P.J., and Goetz, A.F.H. (1993) The spectral image processing system (SIPS)—interactive visualization and analysis of imaging spectrometer data. *Remote Sensing of Environment* 44:145–163.

Langevin, Y., Poulet, F., Bibring, J., and Gondet, B. (2005) Sulfates in the north polar region of Mars detected by OMEGA/Mars Express. *Science* 307:1584–1586.

Lanz, J.K. and Jaurnann, R. (2001) Possible volcanic constructs in Aram Chaos revealed by MOC and their impact on outflow channel genesis [abstract 1574]. In *Proceedings of the 32nd Lunar and Planetary Science Conference,* Lunar and Planetary Institute, Houston.

Maizels, J. (1993) Lithofacies variations within sandur deposits: the role of runoff regime, flow dynamics and sediment supply characteristics. *Sediment. Geol.* 85:299–325.

Mangold, N., Poulet, F., Mustard, J.F. Bibring, J.-P., Gondet, B., Langevin, Y., Ansan, V., Masson, Ph., Fassett, C., Head, J.W., Hoffmann, H., and Neukum, G. (2007) Mineralogy of the Nili Fossae region with OMEGA/Mars Express data: 2. Aqueous alteration of the crust. *J. Geophys. Res.* 112, doi:10.1029/2006JE002835.

Marchenko, A.G., Basilevsky, A.T., Hoffman, H., Hauber, E., Cook, A.C., and Neukum, G. (1998) Geology of the common mouth of the Ares and Tiu Valles, Mars. *Solar System Research* 32:425–452.

Mas, A., Partrier, P., Beaufort, D., and Genter, A. (2003) Clay mineral signatures of fossil and active hydrothermal circulations in the geothermal system of the Lamentin Plain, Martinique. *Journal of Volcanology and Geothermal Research* 124:195–218.

Massé, M., Le Mouelic, S., Bourgeois, O., Combe, J.P., Le Deit, L., Sotin, C., Bibring, J.P., Gondet, B., and Langevin, Y. (2008) Mineralogical composition, structure, morphology, and geological history of Aram Chaos crater fill on Mars derived from OMEGA Mars Express data. *J. Geophys. Res.* 113, doi:10.1029/2008JE003131.

McKenzie, D. and Nimmo, F. (1999) The generation of martian floods by the melting of ground ice above dykes. *Nature* 397:231–233.

McKeown, N.K., Bishop, J.L., Dobrea, E.Z.N., Ehlmann, B.L., Parente, M., Mustard, J.F., Murchie, S.L., Swayze, G.A., Bibring, J.P., and Silver, E.A. (2009) Characterization of phyllosilicates observed in the central Mawrth Vallis region, Mars, their potential formational processes, and implications for past climate. *J. Geophys. Res.* 114, doi:10.1029/2008JE003301.

Meresse, S., Costard, F., Mangold, N., Masson, P., and Neukum, G. (2008) Formation and evolution of the chaotic terrains by subsidence and magmatism: Hydraotes Chaos, Mars. *Icarus* 194:487–500.

Meyer-Dombard, D., Dibbel, A., Bradley, A.S., Shock, E.L., and Summons, R.E. (2007) Microbial diversity and SIP investigations of streamer biofilm communities in Yellowstone National Park. *Geochim. Cosmochim. Acta* 71:A661.

Milliken, R.E. and Mustard, J.F. (2007) Estimating the water content of hydrated minerals using reflectance spectroscopy. I. Effects of darkening agents and low-albedo materials. *Icarus* 189:550–573.

Minitti, M.E., Weitz, C.M., Lane, M.D., and Bishop, J.L. (2007) Morphology, chemistry, and spectral properties of Hawaiian rock coatings and implications for Mars. *J. Geophys. Res.* 112, doi:10.1029/2006JE002839.

Mitrofanov, I.G., Litvak, M.L., Kozyrev, A.S., Sanin, A.B., Tretyakov, V.I., Boynton, W.V., Shinohara, C., Hamara, D., Saunders, S., and Drake, D.M. (2003) Search for water in martian soil using global neutron mapping by the Russian HEND instrument onboard the US 2001 Mars Odyssey spacecraft. *Solar System Research* 37:366–377.

Moore, J.G. (1966) Rate of palagonitization of submarine basalt adjacent to Hawaii. *U.S. Geological Survey Professional Paper* 550-D:163–171.

Moore, D.M. and Reynolds, R.C., Jr. (1997) Identification of clay minerals and associated minerals. In *X-ray Diffraction and the Identification and Analysis of Clay Minerals,* Oxford University Press, New York, pp 203–240.

Morris, A.R. and Mouginis-Mark, P.J. (2006) Thermally distinct craters near Hrad Vallis, Elysium Planitia, Mars. *Icarus* 180:335–347.

Mustard, J.F., Thollot, P., Murchie, S.L., Pelkey, S.M., Ehlmann, B.L., Roach, L.A., Seelos, F., Poulet, F., Bibring, J.P., and the CRISM Science Team. (2007) OMEGA-CRISM characterization of mafic crustal composition: pyroxene [abstract 3230]. In *7th International Conference on Mars,* Lunar and Planetary Institute, Houston.

Mustard, J.F., Murchie, S.L., Pelkey, S.M., Ehlmann, B.L., Milliken, R.E., Grant, J.A., Bibring, J.-P., Poulet, F., Bishop, J., Dobrea, E. Noe, Roach, L., Seelos, F., Arvidson, R.E., Wiseman, S., Green, R., Hash, C., Humm, D., Malaret, E., McGovern, J.A., Seelos, K., Clancy, T., Clark, R., Des Marais, D., Izenberg, N., Knudson, A., Langevin, Y., Martin, T., McGuire, P., Morris, R., Robinson, M., Roush, T., Smith, M., Swayze, G., Taylor, H., Titus, T., and Wolff, M. (2008) Hydrated silicate minerals on Mars observed by the Mars Reconnaissance Orbiter CRISM instrument. *Nature* 454:305–309.

Nelson, D.M. and Greeley, R. (1999) Geology of Xanthe Terra outflow channels and the Mars Pathfinder landing site. *J. Geophys. Res.* 104:8653–8669.

Nelson, M.J., Newsom, H.E., and Draper, D.S. (2005) Incipient hydrothermal alteration of basalts and the origin of martian soil. *Geochim. Cosmochim. Acta.* 69:2701–2711.

Newsom, H.E. (1980) Hydrothermal alteration of impact melt sheets with implications for Mars. *Icarus* 44:207–216.

Orenberg, J. and Handy, J. (1992) Reflectance spectroscopy of palagonite and iron-rich montmorillonite clay mixtures: implications for the surface composition of Mars. *Icarus* 96: 219–225.

Osterloo, M.M., Hamilton, V.E., Bandfield, J.L., Glotch, T.D., Baldridge, A.M., Christensen, P.R., Tornabene, L.L., and Anderson, F.S. (2008) Chloride-bearing materials in the southern highlands of Mars. *Science* 319:1651–654.

Peacock, M.A. (1926) The petrology of Iceland. Part I, The basic tuffs. *Transactions of the Royal Society of Edinburgh* 55:51–76.

Pirajno, F. and van Kranendonk, M.J. (2005) Review of hydrothermal processes and systems on Earth and implications for martian analogues. *Australian Journal of Earth Sciences* 52: 329–351.

Pokrovsky, O.S., Schott, J., Kudryavtzev, D.I., and Dupre, B. (2005) Basalt weathering in Central Siberia under permafrost conditions. *Geochim. Cosmochim. Acta* 69:5659–5680.

Poulet, F., Bibring, J.P., Mustard, J.F., Gendrin, A., Mangold, N., Langevin, Y., Arvidson, R.E., Gondet, B., Gomez, C., and the Omega Team. (2005) Phyllosilicates on Mars and implications for early martian climate. *Nature* 438:623–627.

Poulet, F., Mangold, N., Loizeau, D., Bibring, J.P., Langevin, Y., Michalski, J., and Gondet, B. (2008) Abundance of minerals in the phyllosilicate-rich units on Mars. *Astron. Astrophys.* 487: L41–L44.

Rice, J.W. and Edgett, K.S. (1997) Catastrophic flood sediments in Chryse Basin, Mars, and Quincy Basin, Washington: application of sandar facies model. *J. Geophys. Res.* 102:4185–4200.

Robinson, D. and Santana de Zamora, A. (1999) The smectite to chlorite transition in the Chipilapa geothermal system, El Salvador. *Am. Mineral.* 84:607–619.

Rotto, S. and Tanaka, K.L. (1995) Geologic/geomorphic map of the Chryse Planitia region of Mars. U.S. Geological Survey Miscellaneous Investigations Series Map I-2441, U.S. Geological Survey, Reston, VA.

Roush, T.L. and Bell, J.F., III. (1995) Thermal emission measurements 2000–400 cm^{-1} (5–25 μm) of Hawaiian palagonitic soils and their implications for Mars. *J. Geophys. Res.* 100:5309–5317.

Rowan, L.C. and Mars, J.C. (2003) Lithologic mapping in the Mountain Pass, California area using Advanced Spaceborne Thermal Emission and Reflection Radiometer (ASTER) data. *Remote Sensing of Environment* 84:350–366.

Rowan, L.C., Hook, S.J., Abrams, M.J., and Mars, J.C. (2003) Mapping hydrothermally altered rocks at Cuprite, Nevada, using the Advanced Spaceborne Thermal Emission and Reflection Radiometer (ASTER), a new satellite-imaging system. *Economic Geology and the Bulletin of the Society of Economic Geologists* 98:1019–1027.

Rowan, L.C., Simpson, C.J., and Mars, J.C. (2004) Hyperspectral analysis of the ultramafic complex and adjacent lithologies at Mordor, NT, Australia. *Remote Sensing of Environment* 91:419–431.

Russell, A.J., Knudsen, O., Maizels, J.K., and Marren, P.M. (1999) Channel cross-sectional area changes and peak discharge calculations in the Gígjukvísl river during the November 1996 jökulhlaup, Skeiðarársandur, Iceland. *Jökull* 47:45–58.

Russell, A.J. and Knudsen, O. (2002) The influence of channel flood history on the impact of the November 1996 jökulhlaup, Skeiðarársandur, Iceland. *International Symposium on Extraordinary Floods,* In *The Extremes of the Extremes: Extraordinary Floods,* edited by Snorrason, Finnsdottir, and Moss, International Association of Hydrological Sciences, Wallingford, UK, pp 243–247.

Squyres, S.W., Arvidson, R.E., Ruff, S., Gellert, R., Morris, R.V., Ming, D.W., Crumpler, L., Farmer, J.D., Des Marais, D.J., Yen, A., McLennan, S.M., Calvin, W., Bell, J.F., Clark, B.C., Wang, A., McCoy, T.J., Schmidt, M.E., and de Souza, P.A. (2008) Detection of silica-rich deposits on Mars. *Science* 320:1063–1067.

Stefánsdóttir, M.B. and Gíslason, S.R. (2005) The erosion and suspended matter/seawater interaction during and after the 1996 outburst flood from the Vatnajökull Glacier, Iceland. *Earth Planet. Sci. Lett.* 237:433–452.

Swayze, G.A., Milliken, R.E., Clark, R.N., Bishop, J.L., Ehlmann, B.L., Pelkey, S.M., Mustard, J.F., Murchie, S.L., Brown, A.J., and the MRO CRISM Team. (2007) Spectral evidence for hydrated volcanic and/or impact glass on Mars with MRO CRISM [abstract 3384]. In 7th International Conference on Mars, Lunar and Planetary Institute, Houston.

Tanaka, K.L. (1997) Sedimentary history and mass flow structures of Chryse and Acidalia Planitiae, Mars. J. Geophys. Res. 102:4131–4149.

Thorseth, I.H., Furnes, H., and Tumyr, O. (1991) A textural and chemical study of Icelandic palagonite of varied composition and its bearing on the mechanism of the glass-palagonite transformation. Geochim. Cosmochim. Acta 55:731–749.

Tomasson, H. (1996) The jökulhlaup from Katla in 1918. Annals of Glaciology 22:249–254.

Tosca, N.J. and Knoll, A.H. (2009) Juvenile chemical sediments and the long term persistence of water at the surface of Mars. Earth Planet. Sci. Lett. 286:379–386.

Walter, M.R. and Des Marais, D.J. (1993) Preservation of biological information in thermal spring deposits: developing a strategy for the search for fossil life on Mars. Icarus 101:129–143.

Warner, N.H. and Farmer, J.D. (2008a) The importance of aeolian processes in the origin of Chasma Boreale, Mars. Icarus 196:368–384.

Warner, N.H. and Farmer, J.D. (2008b) The origin of conical mounds at the mouth of Chasma Boreale. J. Geophys. Res. 113, doi:10.1029/2007JE003028.

Williams, D.A., Greeley, R., Werner, S.C., Michael, G., Crown, D.A., Neukum, G., and Raitala, J. (2008) Tyrrhena Patera: geologic history derived from Mars Express High Resolution Camera. J. Geophys. Res. 113 doi:10.1029/2008JE003104.

Wilson, L. and Head, J.W. (2004) Evidence for a massive phreatomagmatic eruption in the initial stages of formation of the Mangala Valles outflow channel, Mars. Geophys. Res. Lett. 31, doi:10.1029/2004GL020322.

Wilson, L. and Mouginis-Mark, P.J. (2003a) Phreato-magmatic dike-cryosphere interactions as the origin of small ridges north of Olympus Mons, Mars. Icarus 165:242–252.

Wilson, L. and Mouginis-Mark, P.J. (2003b) Phreatomagmatic explosive origin of Hrad Vallis, Mars. J. Geophys. Res. 108, doi:10.1029/2002JE001927.

Ylagen, R.F., Altaner, S.P., and Pozzuoli, A. (1996) Hydrothermal alteration of a rhyolitic hyaloclastites from Ponza Island, Italy. Journal of Volcanology and Geothermal Research 74:215–231.

Address correspondence to:
Nicholas H. Warner
Department of Earth Science & Engineering
Imperial College London
South Kensington Campus
London, SW7 2AZ
UK

E-mail: n.warner@imperial.ac.uk